AWARD NUMBER: W81XWH-20-1-0789

TITLE: Pharmacologic Regulation of Auditory Hair Cell Regeneration

PRINCIPAL INVESTIGATOR: Sonia M. Rocha-Sanchez

CONTRACTING ORGANIZATION: Creighton University

TYPE OF REPORT: ANNUAL

REPORT DATE: SEPTEMBER 2021

PREPARED FOR: Creighton University
2500 California Plaza
Omaha, NE 68178

REPORT DOCUMENTATION PAGE

Form Approved
OMB No. 0704-0188

1. REPORT DATE	2. REPORT TYPE	3. DATES COVERED
SEPTEMBER 2021	ANNUAL	1SEPT2020 - 31AUG2021

4. TITLE AND SUBTITLE

Pharmacologic Regulation of Auditory Hair Cell Regeneration

5a. CONTRACT NUMBER
W81XWH-20-1-0789

5b. GRANT NUMBER
RH190008

5c. PROGRAM ELEMENT NUMBER

6. AUTHOR(S)

Sonia M. Rocha-Sanchez

E-Mail: ssanchez@creighton.edu

5d. PROJECT NUMBER

5e. TASK NUMBER

5f. WORK UNIT NUMBER

7. PERFORMING ORGANIZATION NAME(S) AND ADDRESS(ES.)

Creighton University
2500 California Plaza
Omaha, NE 68178

8. PERFORMING ORGANIZATION REPORT NUMBER

9. SPONSORING / MONITORING AGENCY NAME(S) AND ADDRESS(ES.)

US Army Medical Research and Development Command
Fort Detrick, Maryland 21702-5012

10. SPONSOR/MONITOR'S ACRONYM(S)

11. SPONSOR/MONITOR'S REPORT NUMBER(S)

12. DISTRIBUTION / AVAILABILITY STATEMENT

Approved for Public Release. Distribution Unlimited

13. SUPPLEMENTARY NOTES

14. ABSTRACT

Post-mitotic mammalian hair cells (HCs) do not regenerate after traumatic damage, and their death leads to irreversible hearing and balance impairment. Therapeutically induced generation of new sensory HCs has been considered for many years. Nevertheless, there are no available pharmacologic alternatives to stimulate HC regeneration through controlled SC proliferation safely. Studies by our laboratory uncovered the proliferative and therapeutic potential of quinoxaline (Qx), a non-steroidal anti-inflammatory compound to regenerate lost sensorineural HCs. To improve its preclinical properties, we modified our current Qx molecule during the past year, generated several analogs (Qx1 – Qx 70), and tested them *in vitro* and *in vivo* (zebrafish). From those 70 analogs, Qx-27 showed the best medicinal chemistry profile. We have continued to modify that chemotype to expand the structure of activity relationship of this novel chemotype, identify other proliferative analogs, and optimize potency, bioavailability, and *in vivo* efficacy.

15. SUBJECT TERMS
NONE LISTED

16. SECURITY CLASSIFICATION OF:			17. LIMITATION OF ABSTRACT	18. NUMBER OF PAGES	19a. NAME OF RESPONSIBLE PERSON
a. REPORT	b. ABSTRACT	c. THIS PAGE			USAMRMC
Unclassified	Unclassified	Unclassified	Unclassified	50	19b. TELEPHONE NUMBER *(include area*

Standard Form 298 (Rev. 8-98)
Prescribed by ANSI Std. Z39.18

TABLE OF CONTENTS

	Page
1. Introduction	4
2. Keywords	4
3. Accomplishments	4
4. Impact	9
5. Changes/Problems	9
6. Products	10
7. Participants & Other Collaborating Organizations	11
8. Special Reporting Requirements	12
9. Appendices	13

1. INTRODUCTION

Our laboratory characterized a Doxycycline (Dox)-inducible Cyclin D1 (CycD1) overexpression mouse model (*tTA-GFP/TetO-CycD1-Luc/Atoh1-Cre)* (Appendix 1). Results from that study led us to investigate the potential benefits of pharmacologically regulating CycD1 expression via NF-κB signaling to regenerate lost auditory hair cells (HCs) and treat hearing loss. Recent preliminary findings underscored the therapeutic potential of the heterocyclic compound quinoxaline (Qx) (a.k.a. benzopyrazine) - a non-steroidal anti-inflammatory drug - and some of its derivatives to stimulate HC regeneration and to treat hearing loss. Qx has manifold biological properties[1-7]. These diverse activities seem to depend on how it is metabolized within cells (cell-dependent effect), dosage (dose-dependent effect), modifications of its chemical structure, and length of treatment[1-7]. Based upon that premise, we applied medicinal chemistry to (1) improve Qx efficacy in promoting supporting cell (SC) proliferation and differentiation into new HCs and (2) optimize Qx potency for oral delivery. We have generated several analogs (Qx1 – Qx 70) during the past year, which were tested *in vitro* and *in vivo* (zebrafish) for their efficacy to promote supporting cell (SC) proliferation. Based on the results obtained so far, efforts will continue to focus on two series of Qx analogs to expand the structure of activity relationship of this novel chemotype, identify other proliferative analogs, and optimize potency and bioavailability, and *in vivo* efficacy.

References:

1. Moarbess G et al. *Bioorg Med Chem*., 2008;16(13):6601-6610. https://www.ncbi.nlm.nih.gov/pubmed/?term=18513976
2. Cogo J et al. *Eur J Med Chem*., 2015; 90:107-123. https://www.ncbi.nlm.nih.gov/pubmed/25461316
3. Burguete A et al. *Bioorg Med Chem Lett*. 2007; 17(23):6439-6443. https://www.ncbi.nlm.nih.gov/pubmed/17942306
4. Fukushima S et al. *Carcinogenesis*, 2005; 26(11):1835-1845. https://www.ncbi.nlm.nih.gov/pubmed/15975961
5. Fukushima S et al. *Mutagenesis*, 2016;31(3):341-346. https://www.ncbi.nlm.nih.gov/pubmed/26152227
6. Radhakrishnan P et al. *Clin Cancer Res*., 2013;19(8):2025-2035. https://www.ncbi.nlm.nih.gov/pubmed/?term=23444213
7. Kakehashi A et al. *Cancers (Basel)*, 2013;5(4):1332-1354. https://www.ncbi.nlm.nih.gov/pubmed/24202448

2. KEYWORDS

Mammalian auditory hair cells, supporting cells, hearing loss, cell proliferation, cell cycle, hair cell regeneration, medicinal chemistry, drug optimization, quinoxaline, benzopyrazine, NF-κB.

3. ACCOMPLISHMENTS

Despite the global pandemic and limited access to our research facilities, we have made progress during the first year of funding and completed experiments associated with Subtasks 1 and 2, part of the Specific Aim 1 of the original proposal. All tasks completed so far will be described in the following sections of this progress report.

3.1 Major goals of the project

The following are the primary goals of the project:

Specific Aim 1: To improve Qx efficacy in promoting SC proliferation and differentiation into new HCs through medicinal chemistry, structure-activity relationship (SAR), and *in vivo* pharmacokinetics (PK), and pharmacodynamics (PD).	**Projected Completion Time (in months)**	**Percentage of Completion**
Major Task 1: To modify Qx structure and Generate new analogs with improved therapeutic potential		
Subtask 1: To obtain Qx analogs with the following pharmacologic characteristics: 1. IC_{50} lower than the original Qx's IC_{50} (ideally in the nM range).	1-6	80

2. Water solubility at pH 7.4 and stability in solution with $t_{1/2}$ >4 hours. And 3. Show a balance between IC_{50}, potency, efficacy, and ADMET parameters (i.e., absorption, distribution, metabolism, excretion, and toxicity). Optimal Qx analogs will be obtained by the SAR catalog (employing structure databases: ChEMBL, GOSTAR, SciFinder, etc.) and analog synthesis by conventional medicinal chemistry.		
Subtask 2: *In vivo* testing of Qx's top analogs. A pilot study carried out using zebrafish to determine the concentration range of the analogs	7-10	50
Subtask 3: To test Qx top analogs' potency (IC_{50}) and toxicity (LD_{50}) in mouse cochlear explants.	7-14	20
Subtask 4: *In vivo* Pharmacodynamics (PD) and Pharmacokinetics (PK) assessments	7-18	0
Milestone(s) Achieved: Generation and identification of new Qx analogs that meet the pharmacologic characteristics defined above with effective proliferative effects in vitro and in vivo.	18	0
Specific Aim 2: Optimize a Qx's oral delivery method to stimulate HC regeneration and characterize its PK/PD properties in the mouse cochleae.		
Major Task 2: To identify the best oral dosage for Qx, which will result in quantifiable inner ear distribution, lead to safer and controlled cell proliferation, and support the design of preclinical and clinical testing		
Subtask 1: Randomized PD assessment of multiple concentration, single oral dose Qx treatment in normal-hearing mice	18-20	0
Subtask 2: Randomized PK assessment of best oral dose determined on subtask 1, at 0.5, 1, 2, 8- and 24-hours post administration	19-24	0
Milestone(s) Achieved: Identification of optimal oral Qx concentration, which will lead to a consistent and quantifiable proliferative response	24	0

3.2 Current accomplishments under proposed goals

We have designed and conducted experiments described on Specific Aim 1 of our original proposal during the past year. Specifically, we have modified our original Qx molecule to generate several new analogs. The analogs were tested *in vitro* (HEI-OC1 cells). Those showing the selection properties (i.e., IC_{50} lower than original Qx's IC_{50}, Water solubility at pH 7.4 and stability in solution with $t_{1/2}$ >4 hours, and showing a balance between IC_{50}, potency, efficacy, and ADMET parameters) were tested *in vitro* (cochlear explants) and *in vivo* (zebrafish). We describe the major activities, specific objectives, key outcomes, and other achievements of this study in the following sections:

Major Task 1/ Subtask 1: *Design and Synthesis of new Qx analogs* – Qx is an attractive core in medicinal chemistry. Structure-wise, it is an isostere of quinoline (N for C) and naphthalene (2N for 2C), while it is a bioisostere of quinazoline, indole, benzimidazole, benzothiophene, and benzothiazole. Qx-containing compounds can bind to various targets, which makes them a privileged structure. Examples of marketed drugs bearing quinoxaline include the antileprotic clofazimine, the smoking cessation aid varenicline, the antitumor antibiotic phenazinomycin, the antitumor erdafitinib (inhibitor of fibroblast growth factor receptor; FGFR), and the α-adrenergic abrimonidine[8].

Specific Objective: To develop an improved Qx formulation with better pharmacological characteristics (as specified in the table above) than the original Qx formulation.

Key Outcomes: To investigate the influence of the nature of the substituents (R) on Qx biological activity, we generated a series of quinoxaline derivatives by the addition of various R groups ranging from hydrophilic to lipophilic (**Figure 1**). After cooling, the precipitate for each of the 70 compounds

was filtrated and purified by silica gel column chromatography, eluting with heptane (i.e., EtOAc mixture) or methanol in chloroform gradient, and purified by flash column chromatography (**Figure 2**). Final compounds were isolated as solids in moderate yields, usually ranging from 24% to 90% (after all purification steps). All prepared compounds passed PAINS and Aggregators screening using ZINC15 utility (http://zinc15.docking.org/patterns/home; accessed on Jan 15, 2021).

Reference:

8. Bouz G et al. *Pharmaceuticals*, 2021; 14(8): 768. https://doi.org/10.3390/ph14080768

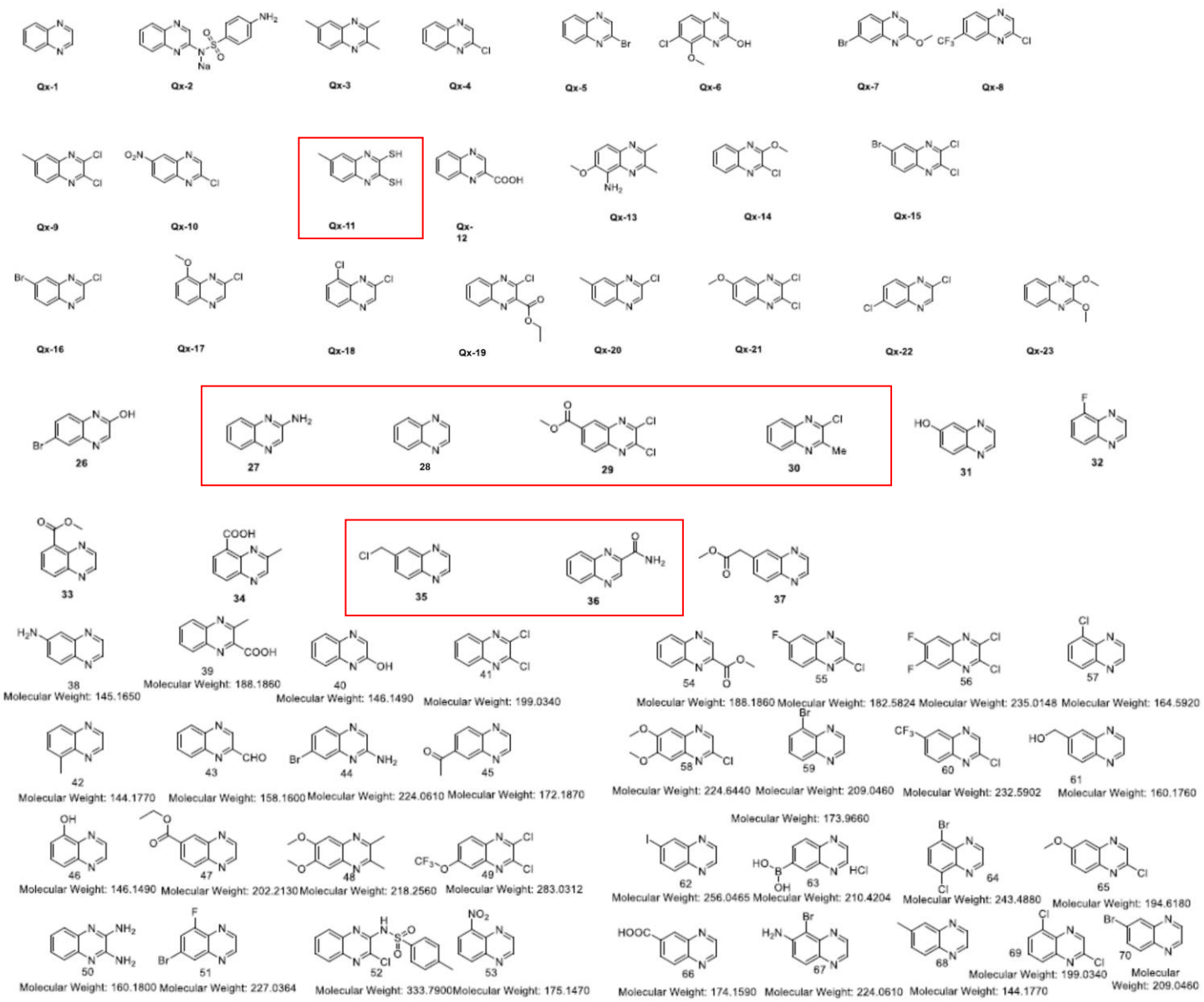

Figure 1. *Chemical structure of Qx derivatives generated in the first phase of the study. The boxed structures represent the chemotypes selected for the subsequent phases of the study.*

Within the 70 different analogs generated, seven chemotypes: Qx-11, Qx-27, Qx-28, Qx-29, Qx30, Qx-35, and Qx-36 showed potential for further improvements (**Figure 3**). Among those, Qx-27 (**Figure 3**; red box) displayed the best pharmacological characteristics (i.e., IC_{50} lower than 25µm, water solubility at pH 7.4, and stability in solution with $t_{1/2}$ >4 hours) and was selected for all subsequent modifications. Of note, Qx-28 (**Figure 3**) was initially considered for further modification but abandoned due to its high instability in solution (data not shown).

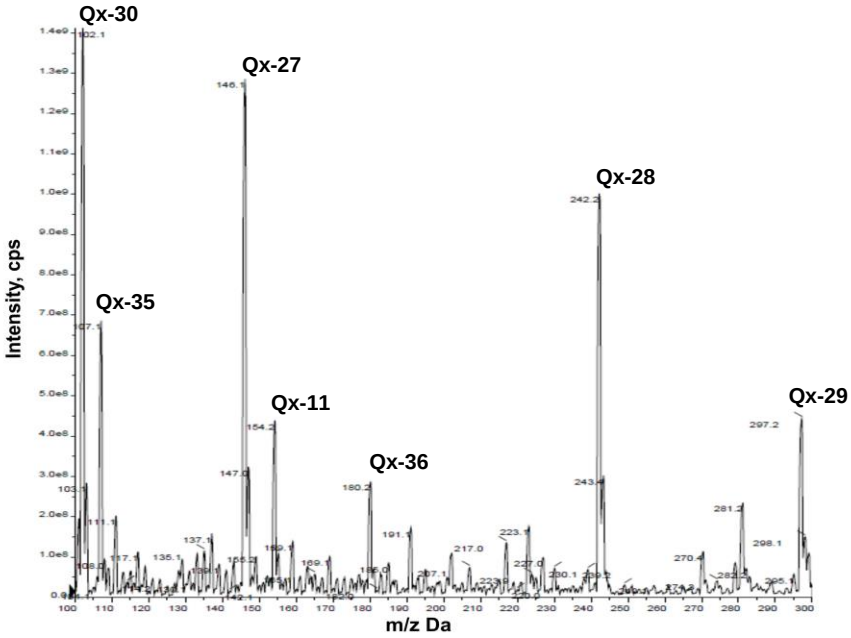

Figure 2. *Purification of the top seven Qx analogs by silica gel column chromatography. cps = counts per second. m/z Da = mass spectrum in Daltons.*

Major Task 1/ Subtasks 2: *In vivo test of Qx top analogs* – Qx elicits otoprotective and proliferative effects in zebrafish[59].

Specific Objective: To further develop and improve the structure-activity relationships of Qx.

Key Outcomes: *In vivo test* - Zebrafish larvae expressing HC membrane-bound GFP (*Tg(brn3c: GFP)*) were incubated with the top seven Qx-derivatives (**Figures 2, 3**). A pilot study of 5 larvae per concentration (300µM and 1µM) of the different Qx analogs (**Figure 4**) helped us determine the range of working dilutions for each candidate and their toxicologic and solubility properties. Qx-27 provided the best proliferative response, at the lowest dose tested with no quantifiable toxicity. This response, combined with its overall performance *in vitro,* led us to select it for further modifications and improvements.

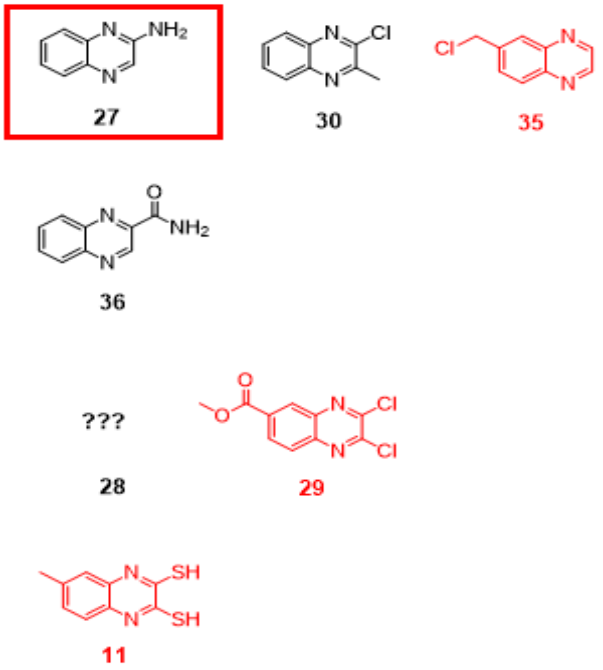

Figure 3. *Top Qx analogs selected among the 70 different chemotypes generated in the first phase of the study.*

Major Task 1/ Subtasks 2/ Major Activity 2:

Further Modification of Qx27 (2-aminoquinoxaline) – Qx-27 is a potent small molecule analog of our lead proliferative drug, Qx. It is a synthetically tractable small molecule ideal for further preclinical optimization.

Specific Objective: To expand the structure of activity relationships of Qx27, identify other otoproliferative analogs, optimize potency, and assess its bioavailability and efficacy *in vitro* and *in vivo*.

Key Outcomes: We focused on designing an alkyl Qx27 series. Alkyl groups include short-chain linear aliphatic chains and heterocycloaliphatic rings. **Figure 5** shows the synthesis of the alkylated Qx27 analogs.

Briefly, 2-chlorquinoxoline is converted to an alkylated Qx27 analog using 2-chloroquinoxaline, various amines, and potassium carbonate in water heated to 105°C in a sealed pressurized flask overnight. After cooling to room temperature, the precipitate is filtered, washed with cold deionized

water, and dried over desiccant overnight. Final products were isolated using normal-phase flash column chromatography (See **Figure 2** for reference). Ten alkylated Qx-27 analogs (Qx-292 – Qx-301) were synthesized and isolated (**Figure 5**). All compounds, except for Qx-297, 298, and 299, were purified using ethyl acetate in hexane gradient. Compounds 297, 298, and 299 were purified using methanol in chloroform gradient. Alkylated Qx-27 analogs were molecularly characterized using mass spectrometry and proton (^{1}H) nuclear magnetic resonance (Data not shown).

Major Task 1/ Subtasks 3: Test of *alkylated Qx27 Analogs* - Alkylated Qx27 elicit proliferative responses in HEI-OC1 Cell Line and in mouse cochlea explant.

Specific Objective: To evaluate the proliferative efficiency of the ten alkylated Qx-27 analogs *in vitro*.

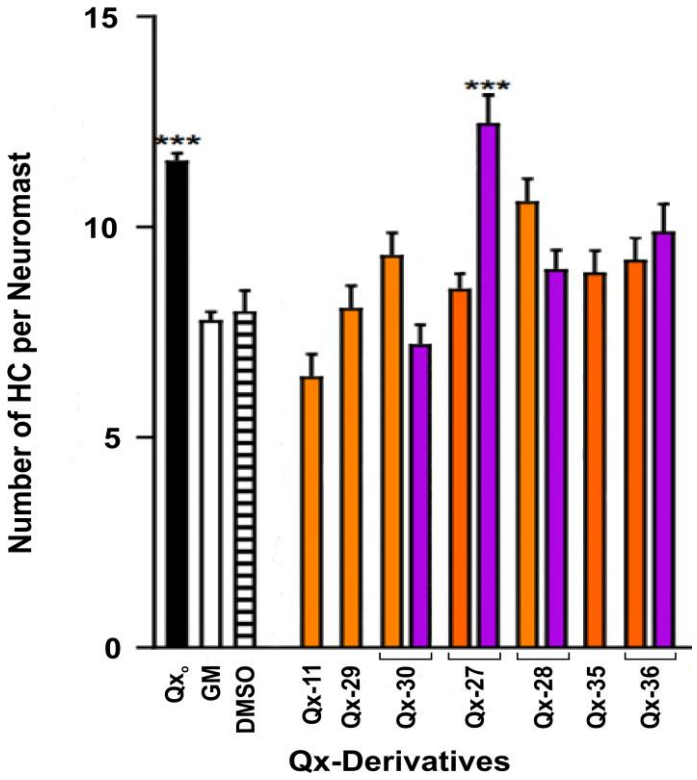

Figure 4. *Scores for neuromast morphology and HC number after treatment with the different Qx analogs. Controls consisted of the original (Qx$_o$) Qx compound, Gentamicin (GM) (negative), and DMSO (negative). Qx-11, Qx-29 and Qx-39 showed no significant proliferative effects at 1µM and were not tested at the lowest concentration (300 µM).* = 1µM; = *300 µM.*

Key Outcomes: All analogs were evaluated against the HEI-OC1 cell line to determine their effect on cell proliferation and cytotoxicity. Five of these compounds were able to show significant and reproducible proliferative effects greater than that of the original Qx (Qx$_o$) and the DMSO controls (**Figure 6**). They were: Qx-292 (ethyl-substituted), Qx-294 (morpholine-substituted), Qx-295 (thiomorpholine-substituted), Qx-296 (acetyl piperazine-substituted), and Qx-**301** (pyrrolidine-substituted).

The ethyl-substituted (Qx-292) showed the highest proliferative effects and over 300% cell viability at 0.5 µM. However, its proliferative effect declined, and it began to show cytotoxic effects at concentrations higher than 1 µM. The compounds Qx-294, Qx-295, Qx-296, and Qx-301 showed over 400% cell viability at all concentrations tested. Nevertheless, their proliferative activity declined at concentrations higher than 5 µM. Notably, all four compounds demonstrated excellent proliferative profiles at concentrations ranging between 100 nM – 5 µM, supporting their high efficiency and safe pharmacological profiles. Altogether, these results endorse further development of alkylated Qx27 analogs as otoproliferative agents with translational potential.

Currently, we are in the process of testing the alkylated Qx-27 compounds in mouse cochlea explants and zebrafish. Due to limited access to the animal research facility and the animals (mice and

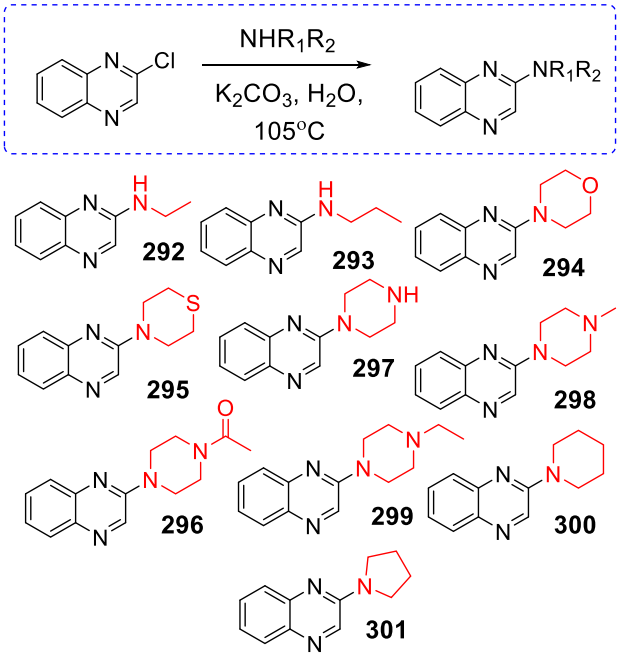

Figure 5. *Synthesis of alkylated Qx27 analogs.*

fish) in the past year, the results obtained so far are still too preliminary to present.

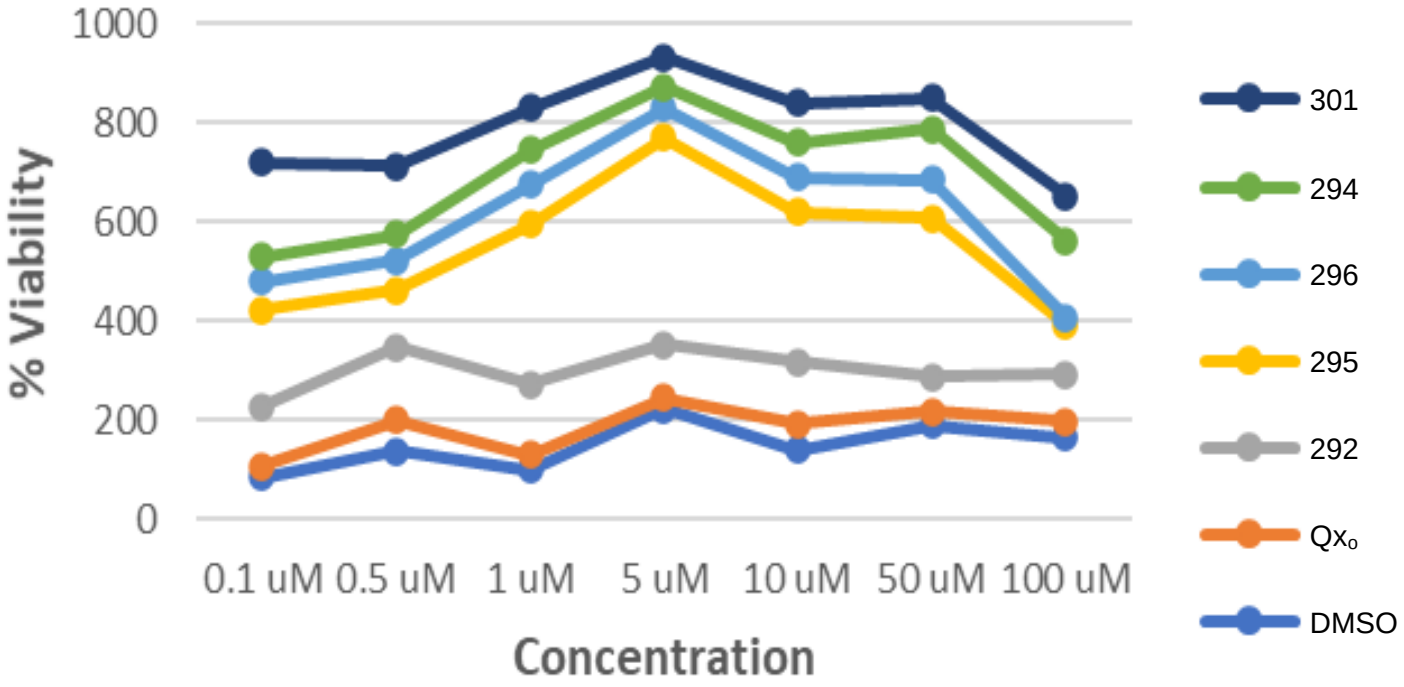

Figure 6. *Proliferative profile of alkylated QX-27 derivatives on HEI-OC1 cells. Controls consisted of the original Qx compound (Qx_o) and DMSO.*

3.3 Opportunities for training

Nothing to report

3.4 Disseminating the results to the community of interest

Nothing to report

3.5 Plans for next reporting period

Despite the difficulties with the pandemic shutdown and limited access to the different research facilities, we have stayed relatively on time with our working plan. Specifically, we have successfully modified the original Qx formulation to generate five new analogs with IC_{50} lower than the original compound. Presently, we are working on further modifications to:

- Improve the new compounds' water solubility, $t_{1/2}$, and ADMET parameters. To accomplish these goals, we plan on continuing and expanding the *in vitro* and *in vivo* experiments, and, upon selection of the top chemotypes, proceed to the pharmacodynamics (PD) and pharmacokinetics (PK) studies and completion of Specific Aim 1, focused on the improvement of Qx_o efficacy through medicinal chemistry. Simultaneously with the completion of Specific Aim 1, we plan to carry out all the studies associated with Specific Aim 2, which is a smaller aim focused on optimization of the new Qx analogs' oral delivery.

- In addition to the limited access to our research facilities, another major drawback was gaining access to the PD and PK laboratories at the other fee-per-services facilities listed in our original application, which were unavailable during the past year. As these facilities are starting

to reopen, we will resume our original plan and proceed to the completion of both PD and PK studies.

4. IMPACT

4.1 Impact on the development of the principal discipline(s) of the project

Nothing to report

4.2 Impact on other disciplines

Nothing to report

4.3 Impact on technology transfer

Nothing to report

4.4 Impact on Society beyond science and technology

Nothing to report

5. CHANGES/PROBLEMS

5.1 Changes in approach and reasons for change

The university shut down and limited access to several research facilities for most of last year have limited our progress; however, no changes have been made to our original research plan.

5.2 Actual or anticipated problems or delays and actions or plans to resolve

Our biggest obstacle was the COVID-19 pandemic. Since the beginning of the pandemic, we have followed the university's guidelines to access the different research facilities, which has caused some delays to the original work plan. Our plan of action, which is already in motion, has consisted of regaining access to facilities that have been completely closed or functioning under restricted hours and make up for the lost time.

5.3 Changes that had a significant impact on expenditures

In October of last year, Dr. Shikha Tarang and Dr. Pavan Kumar Prathipati (Post-Doctoral fellows) left the laboratory to start new positions elsewhere. Moreover, early in March, our laboratory technician left. Since then, I have hired a new full-time laboratory technician, paid out of internal grant funding. During this same time, I have personally taken over the work conducted by Drs. Tarang and Prathipati. These changes have allowed me to save some money on personnel. However, the cost of laboratory supplies and the fee-per-service in some of the research facilities we will use have increased significantly. Therefore, the savings in personnel will make up for the increase in supplies' costs.

5.4 Significant changes in use or care of human subjects, vertebrates, animals, biohazards, and/or select agents

No changes to report

6. PRODUCTS

6.1 Publications, conference papers, and presentations

6.1.1 Journal publications

Rocha-Sanchez SM*, Tarang S., Pyakurel U., Weston, M., Vijayakumar S., Jones T.A., Wagner K-U. (2020) Spatiotemporally Controlled Up-regulation of Cyclin D1 Triggers Generation of Supernumerary Cells in the Postnatal Mouse Inner Ear. *Hearing Res*. doi: 10.1016/j.heares.2020.107951. PMCD: 32244147. (Appendix 1)

6.1.2 Books or other non-periodical, one-time publications

Nothing to report

6.1.3 Other publications, conference papers, and presentations

Rocha-Sanchez S., Pyakurel U., Tarang S., Hati S., Taylor H., He D Z, Liu H., Zuo J., Zallocchi M. (2020) Quinoxaline, its Derivatives, and Application in Otoprotection. 2020 ARO MidWinter Meeting, San Jose, CA. (Appendix 2)

Zallocchi M., Zuo J., Hati S., **Rocha-Sanchez S.**, Pyakurel U., Tarang S. (2020) Quinoxaline protects hair cells from noise-induced damage. 2020 ARO MidWinter Meeting, San Jose, CA. (Appendix 3)

6.2 Website(s) or other Internet sites

Nothing to report

6.3 Technologies or techniques

Nothing to report

6.4 Invention, patent applications, and/or licenses

Nothing to report

6.5 Other Products

Nothing to report

7. Participants and Other Collaborating Organizations

7.1 Project Personnel

Name:	Sonia Rocha-Sanchez
Project Role:	Principal Investigator
Research Identifier:	https://orcid.org/0000-0001-5119-3891
Nearest person month worked:	12
Contribution to project:	Dr. Sanchez has performed work in drug design, testing, and data analyses.
Funding Support:	This award

Name:	Shikha Tarang
Project Role:	Molecular Biologist
Research Identifier:	https://www.linkedin.com/in/shikha-tarang-0642b339/
Nearest person month worked:	1
Contribution to project:	Dr. Tarang performed early *in vitro* drug testing associated with the study
Funding Support:	This award

Name:	Pavan Kumar Prathipati
Project Role:	Medicinal Chemist
Research Identifier:	https://www.linkedin.com/in/pavan-kumar-prathipati-a758b923/
Nearest person month worked:	1
Contribution to project:	Dr. Prathipati helped in the early design of the new Qx chemotypes associated with the study
Funding Support:	This award

Name:	Ross Negrete
Project Role:	Laboratory technician
Research Identifier:	https://www.linkedin.com/in/ross-negrete-969644212/
Nearest person month worked:	7
Contribution to project:	Mr. Negrete performed a variety of general tasks (animal care and handling, lab bench work, ordering, etc.) associated with the study
Funding Support:	Creighton University School of Dentistry Internal Funding

Name:	Lilian Calisto
Project Role:	Laboratory technician
Research Identifier:	https://www.researchgate.net/profile/Lilian-Calisto
Nearest person month worked:	5
Contribution to project:	Ms. Calisto performed a variety of general tasks (animal care and handling, lab bench work, ordering, etc.) associated with the study
Funding Support:	Creighton University School of Dentistry Internal Funding

7.2 Has there been a change in the active other support of the PD/PI(s) or senior/key personnel since the last reporting period?

Nothing to report

7.3 What other organizations were involved as partners?

Nothing to report

8. SPECIAL REPORTING REQUIREMENTS

8.1 Collaborative Awards

Nothing to report

8.2 Quad Charts

Appendix 4

Appendices

Appendix 1

HHS Public Access

Author manuscript

Hear Res. Author manuscript; available in PMC 2021 May 01.

Appendix 1

Published in final edited form as:

Hear Res. 2020 May ; 390: 107951. doi:10.1016/j.heares.2020.107951.

Spatiotemporally controlled overexpression of Cyclin D1 triggers generation of supernumerary cells in the postnatal mouse inner ear

Shikha Tarang[1], **Umesh Pyakurel**[1], **Michael D. Weston**[1], **Sarath Vijayakumar**[2,#], **Timothy Jones**[2], **Kay-Uwe Wagner**[3,$], **Sonia M. Rocha-Sanchez**[1,*]

[1]Creighton University School of Dentistry, Dept. of Oral Biology, Omaha, NE, USA - 68178

[2]University of Nebraska-Lincoln, Dept. of Special Education and Communication Disorders, Lincoln, NE 68583-0738

[3]Professor, University of Nebraska Medical Center, Eppley Institute for Research in Cancer and Allied Diseases, Omaha, NE, USA - 68198

Abstract

The retinoblastoma family of pocket proteins (pRBs), composed of Rb1, p107, and p130 are negative regulators of cell-cycle progression. The deletion of any individual pRB in the auditory system triggers hair cells' (HCs) and supporting cells' (SCs) proliferation to different extents. Nevertheless, accessing their combined role in the inner ear through conditional or complete knockout methods is limited by the early mortality of the triple knockout. In quiescent cells, hyperphosphorylation and inactivation of the pRBs are maintained through the activity of the Cyclin-D1-cdk4/6 complex. Cyclin D1 (CycD1) is expressed in the embryonic and neonatal inner ear. In the mature organ of Corti (OC), CycD1 expression is significantly downregulated, paralleling the OC mitotic quiescence. Earlier studies showed that CycD1 overexpression leads to cell-cycle reactivation in cultures of inner ear explants. Here, we characterize a Cre-activated, Doxycycline (Dox)-controlled, conditional CycD1 overexpression model, which when bred to a tetracycline-controlled transcriptional activator and the *Atoh1-cre* mouse lines, allow for transient

[*]Corresponding author: Sonia M. Rocha-Sanchez, Creighton University School of Dentistry, Dept. of Oral Biology 780729 California Plaza, Omaha, NE 68178-0731, Phone: 402-280-5098, Fax: 402-280-5094, ssanchez@creighton.edu.
[#]Present address: Creighton University, Dept. of Biomedical Sciences, Omaha, NE, USA - 68178
[$]Present address: Wayne State University School of Medicine, Dept. of Oncology, Barbara Ann Karmanos Cancer Institute, Detroit, MI, USA - 48201

Author Contributions

SMR-S designed and oversaw the conduction of the experiments. ST and UP performed the experiments. ABR/DPOAE studies, data analyses, and related figures were prepared by SV and TJ. K-UW provided Cyclin D1 mice and helped with luciferase assay. ST, SMR-S wrote the manuscript. UP, MW, SV, TJ, K-UW discussed the results, helped with data analyses and did a critical revision of the article before submission. All authors have approved the final article.

Declarations of Interest

None

Author Agreement

All authors have seen and approved the final version of the manuscript being submitted.

CycD1 overexpression and pRBs' downregulation in the inner ear in a reversible fashion. Analyses of postnatal mice's inner ears at various time points revealed the presence of supernumerary cells throughout the length of the cochlea and in the vestibular end-organs. Notably, most supernumerary cells were observed in the inner hair cells' (IHCs) region, expressed myosin VIIa (M7a), and showed no signs of apoptosis at any of the time points analyzed. Auditory and vestibular phenotypes were similar between the different genotypes and treatment groups. The fact that no significant differences were observed in auditory and vestibular function supports the notion that the supernumerary cells detected in the adult mice cochlea and macular end-organs may not impair auditory functions.

Keywords

Retinoblastoma; cell-cycle; cyclin D1; supernumerary cells

1. Introduction

The mammalian inner ear sensory epithelia, the organ of Corti (OC), consist of the sensory hair cells (HCs) and their clonally-related supporting cells (SCs). The sensory HCs, which convert mechanical stimuli into electrical signals, are organized into three rows of outer hair cells (OHCs) and one row of inner hair cells (IHCs)[1,2]. Unlike non-mammalian vertebrates, mammals are born with a limited number of HCs, which, when lost, cannot be naturally replaced[3–6]. Loss of sensory HCs leads to permanent and irreversible hearing and balance deficits[3].

Recent studies on HCs' and SCs' cell-cycle regulation have provided new insights into the regenerative potential in the mammalian inner ear[4,7–9]. Mammalian HCs' progenitor cells proliferate during embryogenesis, exit the cell-cycle, differentiate, and become functionally mature after birth[10]. Post-mitotic HCs are unable to re-enter the cell-cycle and are generally referred to as 'quiescent cells'[9]. This post-mitotic quiescence is maintained by the activity of several negative cell-cycle regulators. Consistent with that, loss of cyclin-dependent kinases (CDKs) and some of their inhibitors (e.g., $p27^{Kip1}$, p21Cip1/p19Ink4d) in the postnatal mouse OC, causes HCs and SCs to re-enter the cell cycle, proliferate, and differentiate[4,11–15]. However, as expected from permanently deleting critical regulators of the OC post-mitotic homeostasis[16], these manipulations lead to apoptosis[4,11,12,17–19]. Similar to the CDKs and their inhibitors, the loss of any member of the retinoblastoma (pRB) family, namely *Rb1*, p107, and p130, has been shown to stimulate cell proliferation and differentiation in the postnatal mouse OC[8,16,20–22]. In their role as bona fide cell-cycle inhibitors, these three proteins actively interact with and repress the transcription of genes that are important for HCs and SCs proliferation and differentiation[16]. Interestingly, while *Rb1* deletion is followed by massive cell proliferation and apoptosis[20–22], the deletion of either p107 or p130 results in only mild cell proliferation, without any immediate signs of apoptosis[8,16]. In all cases reported so far, the common denominator of the apoptotic death seems to be the complete and permanent inactivation of genes that are essential for the OC homeostasis.

In almost every cell in our body, cell-cycle progression is dependent on the interaction between the pRBs and Cyclin D1 (CycD1). While pRBs limit proliferation by arresting cells in the G1 to S transition of the cell-cycle, CycD1 removes the pRBs' growth inhibitory function through *G1-Cyclin D-dependent kinase*-mediated phosphorylation[23,24]. Accordingly, pRBs are maintained in an inactive (hyperphosphorylated) state in cells with increased *CycD1-cdk4/6* activity[23,24]. Indeed, the nearly universal detection of mutations in components of this pathway has led to the assumption that disabling the *CycD1-Cdk4/6-Rb1* path may be required for the initiation of unscheduled proliferation in otherwise quiescent cells[23,24]. Correspondingly, CycD1 is upregulated in the developing and neonatal OC[25] when SCs have been shown to re-enter the cell-cycle upon stimulation with exogenous mitogens[26–28]. In the mature OC, the CycD1 expression is significantly downregulated, paralleling OC permanent mitotic quiescence[25]. Moreover, CycD1 overexpression elicits cell-cycle reactivation in inner ear explants[25]. To test whether transient CycD1 overexpression in the postnatal inner ear would overcome the OC mitotic quiescence and trigger proliferation and differentiation of new HCs without inducing apoptosis, we combined the Doxycycline (Dox)-inducibility of a *CAG-βgeo-tTA-GFP*[29] with a CycD1 overexpression model[30], and the *Atoh1-Cre* mouse[31] to generate an inducible *Atoh1-Cre; CAG-βgeo-tTA-GFP;TetO-CycD1-Luc (ACTTD1)*, which allow for CycD1 overexpression and, consequently, controlled and transient downregulation of all three pRBs in the mouse inner ear. Analyses of postnatal mice inner ears at various time points revealed the presence of supernumerary cells throughout the length of the cochlea and in the vestibular end-organs. Most supernumerary cells were located around the IHCs, showed signs of differentiation (e.g., the presence of apical stereocilia, expressed HC differentiation markers, and peripheral innervation), and were still observed in the auditory sensory epithelia at postnatal (P) day 48, the oldest time point examined in this study. To date, there are no effective strategies and products to promote proliferation and safe regeneration of lost auditory HCs. The present study underscores a molecular pathway of potential importance for HC regeneration.

2. Materials and methods

2.1 Animals

The generation of *TetO-CycD1-IRES-Luc* and *CAG-βgeo-tTA-IRES-GFP* transgenic strains is described elsewhere[29,30]. To induce CycD1 overexpression in the auditory sensory epithelia, double transgenic *CAG-βgeo-tTA-IRES-GFP/TetO-CycD1-IRES-Luc* mice were bred to *Atoh1-Cre* mice line (B6. Cg-Tg (Atoh1-cre)1Bfri/J: Jaxmice stock number 011104) to generate a triple transgenic *Atoh1-Cre-CAG-βgeo-tTA-IRES-GFP/TetO-CycD1-IRES-Luc* mouse model (Fig 1). Pups were genotyped for: *tTA* (F -GGC TCT AGA GCC TCT GCT AAC C: R -CTT CGC TAT TAC GCC AGC TGG); *TeTO* (F -GGC GGA TGG TCT CCA CTT CGC: R -CCG TCA GAT CGC CTG GAG ACG) and *Cre* (F -GCC TGC ATT ACC GGT CGA TGC AAC GA: R –GTG GCA GAT GGC GCG GCA ACA CCA TT). Tissues from triple-positive *Atoh1-Cre*$^{+}$*-CAG-βgeo-tTA-GFP*$^{+}$*/TetO-CycD1-Luc*$^{+}$ *(ACTTD1)* transgenic mice were harvested at different postnatal (P) ages (P0, P8, P12, P18, P36, and P48). Dox administration in those animals leads to highly effective suppression of *TetO-CycD1-Luc* (Tet-Off). On the other hand, in the absence of Dox, the tTA induces very strong transactivation of the transgene[29]. Therefore, control animals consisted of mice not

carrying the *Atoh1-Cre* transgene (*tTA*$^{+}$*/TetO-CycD1*$^{+}$) or triple transgenic mice (*ACTTD1*) treated with Dox. To turn-off transgene expression, the *ACTTD1* mice were treated with 2 mg/ml Dox in drinking water at P35, as described in our previous studies[32]. Unless otherwise stated for each specific method, a total of six animals per time point, genotype (e.g., ACTTD1 and control), and technique were used in this study. All animals were treated humanely. All procedures performed were approved by the Creighton University Institutional Animal Care and Use Committee (IACUC) protocol number 0852.

2.2 Luciferase assay

Mice were intraperitoneally injected with luciferin (1 mg D-luciferin potassium salt in 0.2 ml 1× PBS) ten minutes before the imaging procedure. Inner ears were dissected out and transferred to a 96-well plate before imaging. The expression of the luciferase reporter gene associated with the *TetO-CycD1* construct was determined using *in vivo* bioluminescence imaging (IVIS200, Caliper Life Sciences, Alameda, CA).

2.3 Histological analyses

Inner ear tissues of *ACTTD1* and control animals were perfused with 4% paraformaldehyde (PFA) in phosphate-buffered saline (PBS), fixed for 72h at 4°C, and decalcified in 0.5M EDTA/PBS, pH 7.4 overnight. Following decalcification, the cochlear neurosensory epithelia, the organ of Corti, was dissected in PBS. The whole-mount immunohistological analysis was performed as previously described[8]. Briefly, OC tissue pieces (apex, middle, and base) were blocked/permeabilized in 5% NGS/0.1% Tween 20 at room temperature for 2–3h. After that, primary antibody incubations -Cyclin D1 (1:200) (Abcam #Ab16663), Myosin VIIa (M7a) (1:300) (Proteus Biosciences #25–6790), and Green Fluorescent Protein (GFP) (1:300) (Thermo Fisher #MA5–15256) were performed overnight at 4°C. On the following day after three washes in PBS, samples were incubated in respective conjugated secondary antibodies (Life Technologies) overnight at 4°C. Next, samples were washed three times in PBS and mounted in prolong anti-fade mounting medium (Life Technologies) containing DAPI. Imaging was done using a Zeiss LSM 800 confocal laser microscope. Quantification of supernumerary cells was performed on 200X images obtained from three different regions (apex, middle, and base) of six *ACTTD1* and control mice cochleae. Statistical comparison between animal groups and time points was carried out using Two-Way Analysis of Variance (ANOVA) with posthoc Bonferroni correction for multiple comparisons. Values are represented as ± standard deviation (SD) of the mean. $P < 0.05$ was considered significant.

2.4 Semithin sections

Inner ear tissues of P0, P16, and P35 male and female *ACTTD1* and control animals were prepared as previously described[8] and cut into 0.5 μm thick sections. Sections were stained with 0.1% toluidine blue (w/v in water) for 3–5sec and analyzed using a Nikon Eclipse 80i microscope.

2.5 Proliferation assay

To label mitotically active cells, a single, subcutaneous injection of the thymidine analog 5-ethynyl-2'-deoxyuridine (Edu) (50 mg/kg) in DMSO was administered to *ACTTD1* and control mice overnight before tissue harvesting. EdU incorporation into DNA of whole-mount cochleae was detected using the Click-iT EdU Alexa 488 Fluor Imaging kit (ThermoFisher Scientific # C10337) and counterstained with DAPI following the manufacturer's instructions and experimental procedures previously described[33]. Samples were imaged using a Zeiss LSM 800 confocal laser microscope.

2.6 Real-time quantitative PCR (RT-qPCR)

Total RNA from two combined otocysts or two cochleae of WT and *ACTTD1* mice and three biological replicates at various time points was isolated using RNasy kit (Qiagen). A total of 2μg RNA per sample was reverse transcribed as described previously[8]. TaqMan PCR assays (Applied Biosystems, StepOne plus system) for *CycD1* was performed in triplicate for each animal group. Relative quantitation of mRNA abundance was normalized to endogenous *β-Actin* using StepOne Software (Applied Biosystems). T-tests were performed on the normalized gene expression values to determine whether differences were statistically significant. A p-value ≤ 0.05 was considered significant.

2.7 Western blotting

ACTTD1 and control tissues (P12) were homogenized in Ripa lysis buffer (ThermoFisher Scientific #89901) with protease inhibitor (ThermoFisher Scientific #88664) using Omni Homogenizers. Lysates obtained from tissues were cleared by centrifugation at 14,000rpm for 20 min at 4°C. The supernatant was used for protein estimation using the Lowrey method (BioRad DC protein assay kit #500–0112). After that, 20μg of protein was resolved on 10% SDS-PAGE and proteins were then transferred to PVDF membranes (Millipore Immobilon-P #IPVH304FO) in a Bio-Rad TransBlot apparatus per the manufacturer's instructions at 100V for 90 min. After incubation in blocking solution, the PVDF membranes were blocked in 5% blocking solution for 2h at room temperature and probed overnight using primary antibodies Cyclin D1 (Abcam #Ab16663), β-Actin (Santa Cruz # AC-15) at 4°C. The membranes were then washed and incubated in appropriate HRP-conjugated secondary antibodies, anti-rabbit (Santa Cruz), and anti-mouse (Santa Cruz) for 1h at room temperature. After washing, peroxidase-bound protein bands were visualized by chemiluminescence using ECL substrate (Pierce, Rockford, IL, USA).

2.8 Functional assessment of auditory and vestibular function

For evoked potentials [auditory brainstem response (ABR) and vestibular sensory evoked potentials (VsEPs)] and DPOAE measures, mice were anesthetized with a ketamine (18 mg/ml) and xylazine (2 mg/ml) solution (5–9 μl per gram body weight injected intraperitoneally). Core body temperature was maintained at 37.0 ± 0.1°C using a homeothermic heating pad system (FHC, Inc., Bowdoin, ME).

2.9 ABR stimulus and stimulus coupling

For ABR testing, tone burst stimuli were generated and controlled using Tucker Davis Technologies (TDT, Gainesville, FL) System III (RX6, PA5 components). Tone bursts at 8, 16, 32, and 41.2kHz had 1.0 ms rise-fall times with 1.0 ms plateau (3 ms total duration) and alternating stimulus polarity. Stimuli for ABR testing were calibrated using a Bruel & Kjaar type 4138 ¼" microphone and Nexus type 2691 conditioning amplifier. Stimuli were calibrated in dB peSPL and presented via high-frequency transducers (TDT SA1 driver, MF1 speakers) coupled at the ear via PE tubing. Auditory stimuli were presented at a rate of 17 stimuli/sec.

2.10 Vestibular stimulus and stimulus coupling

VsEP recordings are based on methods for mice[34] and are briefly described. Linear acceleration pulses, 2 ms duration, were generated and controlled with National Instruments processors and presented to the cranium via a non-invasive spring clip that encircles the head and secures it to a voltage-controlled mechanical shaker. Stimuli were presented along the naso-occipital axis using two stimulus polarities, normal (+Gx axis) and inverted (–Gx axis) at a rate of 17 pulses/sec. Stimulus amplitudes ranged from +6 dB to –18 dB re: 1.0g/ms (where 1g = 9.8 m/s^2) adjusted in 3 dB steps.

2.11 VsEP and ABR recording

Stainless steel wire was placed subcutaneously over the skull at the nuchal crest to serve as the noninverting electrode. Needle electrodes were placed posterior to the left pinna and at the left hip for inverting and ground electrodes, respectively. Traditional signal averaging was used to resolve responses in electrophysiological recordings. The ongoing electroencephalographic activity was amplified (200,000X), filtered (300 to 3000Hz), and digitized (100kHz sampling rate). 256 or 512 primary responses were averaged for each VsEP or ABR response waveform. All responses were replicated. VsEP intensity series were collected beginning at the maximum stimulus level (i.e., +6 dB re: 1.0g/ms) with and without acoustic masking, then descending in 3 dB steps to −18 dB re: 1.0g/ms. A broadband forward masker (50 to 50,000 Hz, 94 dB SPL) was presented during VsEP measurements to verify the absence of cochlear responses[35]. ABR intensity series were collected with a descending series of stimulus levels (5 dB steps) beginning at approximately 110 dB peSPL.

2.12 VsEP and ABR data analysis

VsEP and ABR thresholds were defined as the stimulus level midway between the minimum stimulus level that produced a discernable response and the maximum level where no response was detectable. Thresholds were compared between knockout and wild type controls using analysis of variance (ANOVA).

2.13 DPOAE recording and data analysis

Methods for recording distortion product otoacoustic emissions (DPOAEs) were similar to those previously described[36,37]. Stimuli for DPOAEs were generated and controlled with modules from TDT. Pure tone frequencies (f1, f2, f2/f1 ratio = 1.25), at equal levels (L1 =

L2 = 60 dBSPL), 150 ms duration, were generated with independent sources (TDT RX6 processor) and routed through separate drivers to mix acoustically in the ear canal (via plastic tubing placed securely at the external acoustic meatus). Stimuli were calibrated in a 0.1ml coupler, which simulates the mouse ear canal volume. Stimulus frequencies for the primaries are such that geometric mean (GM = (f1 x f2)0.5) frequencies ranged from 6.0 to 48.5kHz (at least eight frequencies per octave). Ear canal sound pressure levels were recorded with a low noise probe microphone (Etymotic ER 10B+). The microphone output was amplified and input to the TDT RX6 processor for digital sampling, spectral averaging, and fast Fourier transform (FFT). The amplitude of f1, f2, and the cubic difference distortion product (2f1-f2) were measured from the FFT waveform. The noise floor was measured from the amplitudes in the fifth and twelfth frequency bins above and below (±60 and 120 resp.) the 2f1-f2 component. For statistical comparison (ANOVA), the mean DPOAE amplitude across all tested primary frequency pairs was calculated and compared between knockouts and wild-type controls[38]. After auditory and vestibular analyses, cochleae were processed for histological examination of supernumerary cells.

3. Results

3.1 CycD1 and transgenic constructs' expressions in the inner ear

The *ACTTD1* mouse model analyzed in this study was generated through the breeding of the three previously published lines: *Atoh1-Cre*[31], *CAG-βgeo-tTA-GFP*[29], and the *CAG-βgeo-tTA-GFP;TetO-CycD1-Luc*[39] (Fig 1). As a key regulator of the cell-cycle machinery, CycD1 is expressed during the OC development[25]. To further assess its expression in embryonic and postnatal development, we performed a temporal expression analysis of CycD1 transcripts at various embryonic (E) and postnatal (P) time points (*i.e.,* E12.5, E13.5, E14.5, P0, P14, and P35) (Fig 2A). Consistent with its role, CycD1 levels were higher at embryonic time points (when the inner ear sensory epithelium is undergoing mitotic proliferation) and at neonatal stages (when post-mitotic sensory hair cells are still able to proliferate upon mitogenic stimulation). After that, a sharp decline in CycD1 expression was observed postnatally (Fig 2A), when the pRBs, (particularly Rb1 and Rbl1/p130) are upregulated in the auditory sensory epithelia[8]. While the full-spectrum of CycD1 function in the mouse inner ear is unknown, these analyses suggest that post-mitotic quiescence in the mouse OC coincides with CycD1 downregulation.

Like CycD1, *Atoh1-Cre* expression in the auditory system has been previously established[31]. Furthermore, bioluminescence imaging of mice carrying the *TetO-CycD1* transgene showed overexpression of the exogenous CycD1 in many organs of the *TetO-CycD1-Luc*[39]. To confirm expression of the *CAG-βgeo-tTA* transgene in the auditory system, we performed β-galactosidase (β-gal) reaction on dissected *CAG-βgeo-tTA* adult mice ears (Fig 2B–E). Confirming its expression in the auditory system, positive β-gal reaction was observed throughout the OC, particularly in Deiters' cells (DCs), inner (IPCs), and outer pillar (OPCs) cells, in IHCs and their associated SCs (Fig 2C–E). Positive β-gal expression was also observed in OHCs; however, to a lesser degree (Fig 2D, E). Strong β-gal reactivity was also observed in the vestibular sensory epithelia (Fig 2F).

The *CAG-tTA*-mediated transactivation can be completely ablated through the administration of Dox while its subsequent withdrawal lifts the transcriptional block and leads to effective reactivation of *TetO*-regulated target genes[39]. To confirm effective Dox-controlled transactivation of *CAG-tTA-GFP* and test the repressibility of *CycD1* overexpression, dissected cochleae of triple-positive P12, P26, and P48 aged *ACTTD1* mice treated or not with Dox as well as age-matched controls lacking the *Atoh1-Cre* transgene (negative controls), were submitted to bioluminescence analysis (Fig 3A). Confirming the inducibility and prompt responsiveness of the *CAG-tTA* construct and absence of leaky *TetO-CycD1-Luc* transgene expression, positive luciferase activity was detected in non-Dox-treated *ACTTD1* mice cochleae at both P12 and P48 (Fig 3A, lane 1, wells A, D), but not on age-matched, Dox-treated *ACTTD1* animals (Fig 3A, lane 1, wells B, C). Negative control animals displayed no luciferase activity regardless of the absence (Fig 3A, lane 2, wells A, D) or presence (Fig 3A, lane 2, wells B, C) of Dox. To further assess the inducible nature of the construct and its tight Dox-dependent regulation, P21 *ACTTD1* and age-matched control mice were treated with Dox in drinking water for ten consecutive days, followed by 17 consecutive days without Dox. Contrasting with the complete lack of luciferase activity in the presence of Dox (data not shown but see Fig 3A, lane 1, wells B, C), efficient *CAG-tTA* transgene activation was observed at P48 upon removal of Dox treatment (Fig 3A, lane 1, well E). Once more, no changes were observed in age-matched negative control cochleae (Fig 3A, lane 2, well E). These results were further supported by mRNA (Fig 3B), and protein (Fig 3C) quantification analyses, which showed CycD1 overexpression in non-Dox treated *ACTTD1* mice's inner ear.

3.2 Atoh1-Cre-mediated expression of Dox-controlled CycD1 overexpression triggers the generation of supernumerary cells in postnatal ACTTD1 mouse OC

Given CycD1's direct effect on the regulation of the three pRBs, we pursued to understand the potential effects of its overexpression in the *ACTTD1* mouse cochleae at various postnatal time points. Whole-mount cochleae from *ACTTD1* and control animals not carrying the *Atoh1-Cre* transgene and Dox-treated *ACTTD1* animals were assessed for cell proliferation with the thymidine analog EdU (50 mg/kg) and immunohistochemistry with antibodies against the HC marker Myosin VIIa (M7a), and phalloidin (Fig 4A–J). Additionally, to assess the efficiency of *Atoh1-Cre*-mediated recombination and activation of the *CAG-βgeo-tTA-IRES-GFP* cassette[29], immunohistochemistry using an antibody against GFP was also performed (Fig 4D–E). Of note, despite confirmed *ACTTD1* transcriptional activation in embryonic and early postnatal inner ear, a time when endogenous CycD1 is naturally upregulated (Fig 2A)[25], no significant differences were observed in the inner ear morphology and cell numbers between *ACTTD1* and negative control mice up to one week of age (P7; data not shown). Within the second week of postnatal development, however, changes in cell numbers were already visible (Fig 4A–C). Resembling the β*gal* (tTA) expression pattern (Fig 2B–E) and consistent with efficient CycD1 recombination in the OC, GFP-positive (green) cells were observed throughout the length of the *ACTTD1* mouse cochlea at both OHCs and IHCs region (Fig 4A–H). In many instances, clusters of GFP-positive supernumerary cells were found in the *ACTTD1* mouse cochleae, particularly around the IHCs (Fig 4E, F). Consistent with the presence of actin-rich specialization, supernumerary cells in those clusters appeared to be attached by their phalloidin-positive

apical regions (Fig 4F, F'). Detection of GFP-and EdU-positive nuclei in the same region where the supernumerary cells have been observed (Fig. 4G, G') supports the mitotic origin of those cells. Likewise, simultaneous GFP and M7a expression in the postmitotic supernumerary cells (Fig. 4H) further corroborates their origin and ability to express an HC differentiation marker. Noteworthy, while some EdU-positive cells were observed near the OHCs, particularly at the DCs' region, most EdU-positive cells were detected around the IHCs in the inner border cells' (IBCs) and inner phalangeal cells' (IPhCs) regions (Fig 4G, G'). Control animals displayed the standard 3:1 OHC to IHC ratio without any signs of supernumerary cells (data not shown).

3.3 Cell proliferation and survival in the postnatal ACTTD1 mouse inner ear

Previous research has demonstrated the limited, yet quantifiable, potential of neonatal mouse cochlea HCs to proliferate upon proper stimulation. However, this capacity is generally lost around 7–8 days after birth[4,5]. To further explore the possibility of controlled CycD1 overexpression to stimulate cell proliferation in the developed inner ear, we examined the cochleae of *ACTTD1* mice at later postnatal time points. At P14, recombined (GFP^+) cells were abundant and observed throughout the *ACTTD1* mice cochlea (Fig 5A–D'). Like the younger *ACTTD1* mice, supernumerary cells were arranged in clusters scattered throughout the sensory epithelia (Fig 5A–D'). While some supernumerary cells were observed at the OHCs' region, most supernumerary cells were located around the IHCs, at the IBCs' and IPhCs' region (Fig 5A–D). Although not every GFP^+ cell had an associated cluster of supernumerary cells, extra cells were only observed near recombined cells (Fig 5A–D). The GFP-positive nature of the supernumerary cells, along with their distribution in the sensory epithelia, is consistent with them deriving from the IBCs' and IPhCs' cycle re-entry, rather than from the differentiated HCs[40,41] (Fig 5D'–F). Additional lineage tracing analyses is needed to validate this preliminary observation. At P18, only a few proliferative cells were observed scattered throughout different regions of the cochleae (Fig 5F). By P36 and P48, no detectable signs of cell proliferation were observed, yet GFP-and M7a-positive supernumerary cells were still seen in the OC, particularly around the IHCs (Fig 6A–G). Quantification of supernumerary cells in the ACTTD1 cochleae was performed for all four time points analyzed in this study (i.e., P8, P18, P36, and P48) (Fig. 6H). Despite age or cochlear turn (i.e., apex, middle, and base) analyzed, the average number of cells per 100 μm of cochleae was higher in ACTTD1 mice than the control group, which showed no supernumerary cells (data not shown). Within each ACTTD1 age groups, there was an overall higher concentration of supernumerary cells in the apical region ($P < 0.05$) (Fig. 6H), as compared to middle or basal turns, particularly at P8 and P36 ($P < 0.05$) (Fig. 6H). While the trend for a higher number of supernumerary cells in the apical region was still observed at P48, the difference in cell number between turns was not significant (Fig. 6H) at that time point. Comparison between P36 and P48 cochleae showed a significant decrease in supernumerary apical cells ($P < 0.05$) and an increase in cells at the basal turn ($P < 0.05$) (Fig. 6H) at the latter time point. Whether the decrease in supernumerary apical cells was due to cell death or any other factors is not yet clear. Of note, no signs of apoptosis were detected at any time point by TUNEL or Caspase-3 assays (data not shown).

Like the cochlear sensory epithelia, clusters of supernumerary cells, many of which displaying phalloidin-positive apical signals, as well as several mitotic figures, were observed in the postnatal *ACTTD1* mice vestibular end-organs' sensory epithelia (Fig 7A–H). By P48, the latest time point analyzed, supernumerary cells were still present in the vestibular sensory epithelia (Fig 7H). No signs of mitotic proliferation were observed past P18 (Fig 7E–G). Nevertheless, several interphasic cells displaying large nuclei, uncondensed chromatin, and large nucleoli were still observed at the vestibular supporting cells' region at P48 (Fig 7H, arrows).

3.4 Auditory and vestibular assessment of ACTTD1 mouse model

As supernumerary cells persisted in the *ACTTD1* adult mouse inner ear, we pursued to assess the functionality of the cochleae and vestibular systems. Adult animals were divided into three different treatment groups consisting of tTA/TetO-CycD1 not carrying the *Atoh1-Cre* transgene (P33; n = 7), *ACTTD1* mice treated with Dox [*ACTTD1* (+) Dox; P45; n = 4] and the *ACTTD1* experimental group not treated with Dox [*ACTTD1* (−) Dox; P35; n = 5]. VsEPs, ABRs, and DPOAEs were completed for all groups. To confirm the presence of supernumerary cells, cochleae from all animals tested were dissected and submitted to histological analyses (Fig. 6A–H).

3.4.1 Vestibular function—Vestibular (VsEP) thresholds reflect the general sensitivity of the macular epithelium to the transient head motion. Mean VsEP thresholds for all treatment groups were within the normal vestibular sensitivity range (Fig 8A). Overall, there were no significant differences in VsEPs thresholds across treatment groups (data not shown). VsEP amplitudes (p1-n1) reflect the number of primary afferent neurons contributing to the response and the degree to which they are activated synchronously with our transient stimulus. At the highest level of stimulation (+6 dB re:1g/ms), vestibular amplitudes were within the range of amplitudes found in standard laboratory controls (Fig 8B). Like VsEPs thresholds, there were no significant differences in VsEP amplitudes between the three treatment groups (data not shown). The encoding of the stimulus level was explored by evaluating VsEP response amplitudes as a function of stimulus level above threshold (dB SL). There were no differences in p1-n1 amplitudes between treatment groups over the three stimulus levels evidencing the largest stable sample sizes for each group (4.5, 7.5, 10.5 dB SL), thus indicating the usual response characteristics of the macular neural population for treatment groups over a wide range of stimulus levels (Fig 8C). Vestibular latencies (p1, n1) reflect the activation timing associated with sensory transduction in hair cells and subsequent activation of the postsynaptic macular primary afferent neurons responding to our stimulus. At the highest stimulus level, latencies of both p1 and n1 were within the normal limits for laboratory control animals (Fig 8D). There was no significant difference between groups for the first positive peak (p1). However, latencies for the experimental [*ACTTD1* (−) Dox] group were slightly shorter than the tTA/TetO-CycD1 group (mean difference 98.3 microseconds) but not the *ACTTD1* (+) Dox group (MANOVA, post hoc Bonf $P = 0.006$). The *ACTTD1* (+) Dox treatment group showed no differences in latency from control or *ACTTD1* (−) Dox groups. The latency difference between control and *ACTTD1* (−) Dox group disappeared when thresholds were taken into consideration and response latencies expressed in relation to each animals' threshold (dB SL, Fig 8E). There

was a normal relationship between latency and stimulus level above threshold, and there were no significant differences in latency between groups (evaluated over 4.5, 7.5, and 10.5 dB SL levels). Thus, the shorter n1 latency obtained at the highest absolute stimulus level (+6 dB re:1g/ms) in the *ACTTD1* (−) Dox group likely reflects a slightly improved sensitivity for this group.

3.4.2 Auditory Function—There were no significant differences in ABR thresholds at any frequency across all treatment groups (Fig 9A–D). Likewise, the DPOAE-gram suggested relatively normal emission amplitudes from 8 to32 KHz (Fig 9 E). Of note, a marked reduction in emissions above 32 KHz was observed in all three treatment groups. However, based on the uniform response for all three treatment groups, it is unlikely that this reduction in emissions is due to the presence of supernumerary cells.

4.0 Discussion

Previous studies, ours included, have demonstrated that inactivation of any of the endogenous pRB proteins (Rb1, p107, or p130) leads to transient cell proliferation and differentiation, at varied extensions, in the mammalian inner ear[8,16,21,22,42]. However, consistent with each pRB's role in the cell-cycle machinery and cellular homeostasis, newly generated HCs and SCs fail to survive[17,19,21,42], an undesirable outcome for regenerative approaches. The possibility of collectively and transiently suppressing the combined expression of all three pRBs in the mammalian inner ear has been previously considered. However, knockout mice lacking all three pRBs are unviable[43,44]. We sought an approach at cell cycle control that extends this previous work in a novel and innovative way. We developed a system to control Cyclin D1, both spatially and temporally. Cyclin D1 is prominently implicated in the phosphorylation and inactivation of the pRBs: Underphosphorylated pRbs inhibit the cell-cycle progression while hyperphosphorylation of these proteins renders them inactive and allow the cell-cycle to progress[9]. In this light, we sought to investigate the effects of controlled, cell-specific overexpression of CycD1 in the *ACTTD1* mouse inner ear. Under normal circumstances, endogenous CycD1 expression is postnatally downregulated in the mouse OC. However, *ACTTD1* mice displayed high levels of CycD1 expression at time points when CycD1 would be naturally downregulated. Such elevated expression resulted in the presence of supernumerary cells in the postnatal inner ear. Interestingly, considering that CycD1 overexpression was controlled by a Tet-off system, no signs of unscheduled proliferation was observed before P8, when the CycD1 endogenous expression is naturally elevated in the inner ear. In a variety of different systems, the temporal regulation of protein abundance and post-translational modification is a key feature of mitotic proliferation[45–47]. Previous studies on protein phosphorylation dynamics during the cell-cycle have also shown a normal tendency for tight regulation of protein abundance and degradation as a means to maintain a stoichiometric control of their activity[48–50]. As such, an increase in CycD1 synthesis when its expression is already elevated could lead to an increase in the flux of protein degradation[51], resulting in no changes in mitotic proliferation. Nevertheless, as the endogenous CycD1 expression went down, continued activity of the transgenic CycD1 past its normal activity time led to pRBs' hyperphosphorylation and consequential functional inactivation, as reflected by the presence

of supernumerary cells in both cochleae and vestibular end-organs. Interestingly, despite the presence of recombined GFP-positive cells at both the OHCs and IHCs region in the *ACTTD1* mouse cochleae, most cell proliferation was restricted to the IHCs' region, suggesting higher plasticity of cells in that region. This observation is supported by previous studies showing differences in auditory cells' predisposition to unscheduled proliferation[52–54]. While lineage-tracing studies are likely to confirm the origin of those supernumerary cells, evidence collected so far (e.g., detection of GFP expression in recombined and supernumerary cells as well as the physical location of the EdU-positive and supernumerary cells) points out primarily to the IPhCs and IBCs, and DCs, to a lesser extent, as the likely source of supernumerary cells in the *ACTTD1* mouse inner ear. This observation is supported by previous report of *Atoh1-Cre* expression[19,55], the detection of *CAG-βgeo-tTA-IRES-GFP* expression (this study), and the higher proliferative potential of SCs, particularly at the IHCs' supporting cells region. Fine-tuning of the proposed method could potentially open many avenues for the development of HC regenerative strategies. While both hair cell types are essential for hearing, the IHCs are the actual sensory receptors of the cochlea, responsible for detecting and transmitting sound information to the brain. It is estimated that 95% of the afferent auditory nerve fibers projecting to the brain arise from this subpopulation of cells[56]. Although the goal is to achieve complete regeneration of lost auditory hair cells, successful regeneration of IHCs, particularly in older individuals, as suggested by our present findings, can have a significant impact in the field of hearing restoration and open new avenues for the pursuit of regenerative strategies.

ACTTD1 supernumerary cells are organized in characteristic 'flower-like' clusters. Moreover, most of the supernumerary cells displayed actin-rich apical specializations at all time points studied. These characteristics added to the fact that most non-dividing supernumerary cells expressed the HC marker M7a suggest that CycD1 overexpression not only unleashed unscheduled cell proliferation but most, if not all, the supernumerary cells continued to differentiate into HC-like cells. These results are supported by many others, including some of our studies, showing morphological and functional differentiation of supernumerary HCs[25]. Noteworthy, neither the presence nor the clustered organization of the supernumerary cells seems to have impacted auditory function. Like the p130 knockout mouse[8], *ACTTD1* displayed near-normal hearing and vestibular function, despite the presence of supernumerary cells in both cochleae and vestibular sensory epithelia. It is important to highlight that unlike other mammalian vertebrates, human HCs are not organized in straight lines[2,57]. Previous reports have shown that human IHCs can be naturally arranged in small clusters without affecting auditory function[58,59]. Previous studies looking into HC regeneration through gene manipulation, p27kip knockout[6,15,55,60,61], Atoh1-overexpression[54,62–67], Notch signaling downregulation[68–71], deletion of individual members of the retinoblastoma family[8,16,21,22], Hes1/Hes5 modulation[66,72,73] among others have shown that new HCs can be generated through manipulation of different components of the HCs and SCs cell-cycle pathway. However, unlike those previous studies which involved genetic manipulation of cell-cycle genes[4,5], our Cyclin D1 overexpression model modulates downstream pRBs's expression post-translationally, leading to their increased hyperphosphorylation and degradation. So, while the conditional CycD1 upregulation model allows us to transiently downregulate the expression of all three pRBs in a combined

fashion, it also allows for residual protein expression. This strategy allowed cells in *ACTTD1* cell-cycle re-entry at older time points (P8-P18) and remained alive for longer than previously described for other models. No evidence of cell-death was detected, as shown by negative caspase 3 staining and TUNNEL staining.

5.0 Conclusion

The therapeutic potential of the retinoblastoma (pRB) family (i.e., Rb1, Rbl1/p107, and Rbl2/p130) in HC regeneration has been appreciated for many years. However, no approach to date has been effective in allowing for understanding their activity in the auditory system without permanently deleting those crucial genes. The present study addresses such a lack of knowledge on the combined effect of the pRB inactivation in the auditory sensory epithelia and demonstrates that in a controlled system, postnatal auditory SCs can be stimulated to proliferate. The resultant supernumerary cells can survive for an extended period (e.g., P48) without adversely affecting auditory functions. Although preliminary, these findings add to amounting pieces of evidence already available in the literature supporting the potential of targeted and controlled manipulation of the auditory SCs' cell cycle on the development of future regenerative strategies.

Acknowledgments

Technical support for luciferase imaging was provided by Drs. Kazuhito Sakamoto and Qian Zhang (UNMC). The microscopic confocal systems were made available by the UNMC Advanced Microscopy Core facility and Nebraska Center for Cell Biology (NCCB) at Creighton University. Mouse lines used in the study were maintained at Creighton University's Animal Resource Facility. This work received past support through an NIH/NCRR 5P20RR018788-/NIH/NIGMS 8P20GM103471 COBRE grant (Shelley D. Smith, PI) and NIH/ORIP R21OD019745–01A1 (S.M.R.-S.).

References

1. Raphael Y, Altschuler RA. Structure and innervation of the cochlea. Brain Res Bull 2003;60(5–6):397–422. [PubMed: 12787864]
2. Dallos P, Popper AN, Fay RR, eds. Structure of the mammalian cochlea vol 8 ed. New York, NY: Springer,; 1996 10.1007/978-1-4612-0757-3_2.
3. Raphael Y Cochlear pathology, sensory cell death and regeneration. Br Med Bull 2002;63:25–38. [PubMed: 12324382]
4. White PM, Doetzlhofer A, Lee YS, Groves AK, Segil N. Mammalian cochlear supporting cells can divide and trans-differentiate into hair cells. Nature. 2006;441(7096):984–987. [PubMed: 16791196]
5. Cox BC, Chai R, Lenoir A, et al. Spontaneous hair cell regeneration in the neonatal mouse cochlea in vivo. Development. 2014;141(4):816–829. [PubMed: 24496619]
6. Oesterle EC, Campbell S, Taylor RR, Forge A, Hume CR. Sox2 and JAGGED1 expression in normal and drug-damaged adult mouse inner ear. J Assoc Res Otolaryngol 2008;9(1):65–89. [PubMed: 18157569]
7. Schimmang T, Pirvola U. Coupling the cell cycle to development and regeneration of the inner ear. Semin Cell Dev Biol 2013;24(5):507–513. [PubMed: 23665151]
8. Rocha-Sanchez SM, Scheetz LR, Contreras M, et al. Mature mice lacking Rbl2/p130 gene have supernumerary inner ear hair cells and supporting cells. J Neurosci 2011;31(24):8883–8893. [PubMed: 21677172]
9. Rocha-Sanchez SM, Beisel KW. Pocket proteins and cell cycle regulation in inner ear development. Int J Dev Biol 2007;51(6–7):585–595. [PubMed: 17891719]

10. Lee YS, Liu F, Segil N. A morphogenetic wave of p27Kip1 transcription directs cell cycle exit during organ of corti development. Development. 2006;133(15):2817–2826. [PubMed: 16790479]
11. Chen P, Segil N. p27(Kip1) links cell proliferation to morphogenesis in the developing organ of corti. Development. 1999;126(8):1581–1590. [PubMed: 10079221]
12. Laine H, Sulg M, Kirjavainen A, Pirvola U. Cell cycle regulation in the inner ear sensory epithelia: Role of cyclin D1 and cyclin-dependent kinase inhibitors. Dev Biol 2010;337(1):134–146. [PubMed: 19854167]
13. Walters BJ, Liu Z, Crabtree M, Coak E, Cox BC, Zuo J. Auditory hair cell-specific deletion of p27Kip1 in postnatal mice promotes cell-autonomous generation of new hair cells and normal hearing. J Neurosci 2014;34(47):15751–15763. [PubMed: 25411503]
14. Lowenheim H, Furness DN, Kil J, et al. Gene disruption of p27(Kip1) allows cell proliferation in the postnatal and adult organ of corti. Proc Natl Acad Sci U S A 1999;96(7):4084–4088. [PubMed: 10097167]
15. Minoda R, Izumikawa M, Kawamoto K, Zhang H, Raphael Y. Manipulating cell cycle regulation in the mature cochlea. Hear Res 2007;232(1–2):44–51. [PubMed: 17658230]
16. Rocha-Sanchez SM, Scheetz L, Siddiqi S, et al. Lack of *rbl*1/p107 effects on cell proliferation and maturation in the inner ear. Journal of Behavioral and Brain Science. 2013;3(7):534–555.
17. Huang M, Sage C, Tang Y, et al. Overlapping and distinct pRb pathways in the mammalian auditory and vestibular organs. Cell Cycle. 2011;10(2):337–351. [PubMed: 21239885]
18. Weber T, Corbett MK, Chow LM, Valentine MB, Baker SJ, Zuo J. Rapid cell-cycle reentry and cell death after acute inactivation of the retinoblastoma gene product in postnatal cochlear hair cells. Proc Natl Acad Sci U S A 2008;105(2):781–785. [PubMed: 18178626]
19. Yu Y, Weber T, Yamashita T, et al. In vivo proliferation of postmitotic cochlear supporting cells by acute ablation of the retinoblastoma protein in neonatal mice. J Neurosci 2010;30(17):5927–5936. [PubMed: 20427652]
20. Mantela J, Jiang Z, Ylikoski J, Fritzsch B, Zacksenhaus E, Pirvola U. The retinoblastoma gene pathway regulates the postmitotic state of hair cells of the mouse inner ear. Development. 2005;132(10):2377–2388. [PubMed: 15843406]
21. Sage C, Huang M, Karimi K, et al. Proliferation of functional hair cells in vivo in the absence of the retinoblastoma protein. Science. 2005;307(5712):1114–1118. [PubMed: 15653467]
22. Sage C, Huang M, Vollrath MA, et al. Essential role of retinoblastoma protein in mammalian hair cell development and hearing. Proc Natl Acad Sci U S A 2006;103(19):7345–7350. [PubMed: 16648263]
23. Calbo J, Parreno M, Sotillo E, et al. G1 cyclin/cyclin-dependent kinase-coordinated phosphorylation of endogenous pocket proteins differentially regulates their interactions with E2F4 and E2F1 and gene expression. J Biol Chem 2002;277(52):50263–50274. [PubMed: 12401786]
24. Nishi K, Inoue H, Schnier JB, Rice RH. Cyclin D1 downregulation is important for permanent cell cycle exit and initiation of differentiation induced by anchorage-deprivation in human keratinocytes. J Cell Biochem 2009;106(1):63–72. [PubMed: 19021145]
25. Laine H, Sulg M, Kirjavainen A, Pirvola U. Cell cycle regulation in the inner ear sensory epithelia: Role of cyclin D1 and cyclin-dependent kinase inhibitors. Dev Biol 2010;337(1):134–146. [PubMed: 19854167]
26. Gu R, Montcouquiol M, Marchionni M, Corwin JT. Proliferative responses to growth factors decline rapidly during postnatal maturation of mammalian hair cell epithelia. Eur J Neurosci 2007;25(5):1363–1372. [PubMed: 17425563]
27. Montcouquiol M, Corwin JT. Brief treatments with forskolin enhance s-phase entry in balance epithelia from the ears of rats. J Neurosci 2001;21(3):974–982. [PubMed: 11157083]
28. Lu Z, Corwin JT. The influence of glycogen synthase kinase 3 in limiting cell addition in the mammalian ear. Dev Neurobiol 2008;68(8):1059–1075. [PubMed: 18470861]
29. Zhang Q, Triplett AA, Harms DW, et al. Temporally and spatially controlled expression of transgenes in embryonic and adult tissues. Transgenic Res 2010;19(3):499–509. [PubMed: 19821046]

30. Zhang Q, Sakamoto K, Liu C, et al. Cyclin D3 compensates for the loss of cyclin D1 during ErbB2-induced mammary tumor initiation and progression. Cancer Res 2011;71(24):7513–7524. [PubMed: 22037875]
31. Matei V, Pauley S, Kaing S, et al. Smaller inner ear sensory epithelia in neurog 1 null mice are related to earlier hair cell cycle exit. Dev Dyn 2005;234(3):633–650. [PubMed: 16145671]
32. Tarang S, Doi SM, Gurumurthy CB, Harms D, Quadros R, Rocha-Sanchez SM. Generation of a retinoblastoma (rb)1-inducible dominant-negative (DN) mouse model. Front Cell Neurosci 2015;9:52. [PubMed: 25755634]
33. Kaiser CL, Kamien AJ, Shah PA, Chapman BJ, Cotanche DA. 5-ethynyl-2'-deoxyuridine labeling detects proliferating cells in the regenerating avian cochlea. Laryngoscope. 2009;119(9):1770–1775. [PubMed: 19554638]
34. Honaker JA, Lee C, Criter RE, Jones TA. Test-retest reliability of the vestibular sensory-evoked potential (VsEP) in C57BL/6J mice. J Am Acad Audiol 2015;26(1):59–67. [PubMed: 25597461]
35. Jones SM, Erway LC, Bergstrom RA, Schimenti JC, Jones TA. Vestibular responses to linear acceleration are absent in otoconia-deficient C57BL/6JEi-het mice. Hear Res 1999;135(1–2):56–60. [PubMed: 10491954]
36. Guimaraes P, Zhu X, Cannon T, Kim S, Frisina RD. Sex differences in distortion product otoacoustic emissions as a function of age in CBA mice. Hear Res 2004;192(1–2):83–89. [PubMed: 15157966]
37. Jimenez AM, Stagner BB, Martin GK, Lonsbury-Martin BL. Age-related loss of distortion product otoacoustic emissions in four mouse strains. Hear Res 1999;138(1–2):91–105. [PubMed: 10575118]
38. Martin GK, Vazquez AE, Jimenez AM, Stagner BB, Howard MA, Lonsbury-Martin BL. Comparison of distortion product otoacoustic emissions in 28 inbred strains of mice. Hear Res 2007;234(1–2):59–72. [PubMed: 17997239]
39. Zhang Q, Sakamoto K, Liu C, et al. Cyclin D3 compensates for the loss of cyclin D1 during ErbB2-induced mammary tumor initiation and progression. Cancer Res 2011;71(24):7513–7524. [PubMed: 22037875]
40. Lewis RM, Hume CR, Stone JS. Atoh1 expression and function during auditory hair cell regeneration in post-hatch chickens. Hear Res 2012;289(1–2):74–85. [PubMed: 22543087]
41. Yang H, Xie X, Deng M, Chen X, Gan L. Generation and characterization of Atoh1-cre knock-in mouse line. Genesis. 2010;48(6):407–413. [PubMed: 20533400]
42. Weber T, Corbett MK, Chow LM, Valentine MB, Baker SJ, Zuo J. Rapid cell-cycle reentry and cell death after acute inactivation of the retinoblastoma gene product in postnatal cochlear hair cells. Proc Natl Acad Sci U S A 2008;105(2):781–785. [PubMed: 18178626]
43. Maandag EC, van der Valk M, Vlaar M, et al. Developmental rescue of an embryonic-lethal mutation in the retinoblastoma gene in chimeric mice. EMBO J 1994;13(18):4260–4268. [PubMed: 7925271]
44. Wu L, de Bruin A, Saavedra HI, et al. Extra-embryonic function of rb is essential for embryonic development and viability. Nature. 2003;421(6926):942–947. [PubMed: 12607001]
45. Ly T, Whigham A, Clarke R, et al. Proteomic analysis of cell cycle progression in asynchronous cultures, including mitotic subphases, using PRIMMUS. Elife. 2017;6:10.7554/eLife.27574.
46. Naryzhny SN, Lee H. The post-translational modifications of proliferating cell nuclear antigen: Acetylation, not phosphorylation, plays an important role in the regulation of its function. J Biol Chem 2004;279(19):20194–20199. [PubMed: 14988403]
47. Pardee AB. Multiple molecular levels of cell cycle regulation. J Cell Biochem 1994;54(4):375–378. [PubMed: 8014185]
48. Ardito F, Giuliani M, Perrone D, Troiano G, Lo Muzio L. The crucial role of protein phosphorylation in cell signaling and its use as targeted therapy (review). Int J Mol Med 2017;40(2):271–280. [PubMed: 28656226]
49. Buchkovich K, Duffy LA, Harlow E. The retinoblastoma protein is phosphorylated during specific phases of the cell cycle. Cell. 1989;58(6):1097–1105. [PubMed: 2673543]
50. Mayol X, Garriga J, Grana X. Cell cycle-dependent phosphorylation of the retinoblastoma-related protein p130. Oncogene. 1995;11(4):801–808. [PubMed: 7651744]

51. Alao JP. The regulation of cyclin D1 degradation: Roles in cancer development and the potential for therapeutic invention. Mol Cancer. 2007;6:24-4598-6-24.
52. Kuo BR, Baldwin EM, Layman WS, Taketo MM, Zuo J. In vivo cochlear hair cell generation and survival by coactivation of beta-catenin and Atoh1. J Neurosci 2015;35(30):10786–10798. [PubMed: 26224861]
53. Liu Z, Dearman JA, Cox BC, et al. Age-dependent in vivo conversion of mouse cochlear pillar and deiters' cells to immature hair cells by Atoh1 ectopic expression. J Neurosci 2012;32(19):6600–6610. [PubMed: 22573682]
54. Liu Z, Fang J, Dearman J, Zhang L, Zuo J. In vivo generation of immature inner hair cells in neonatal mouse cochleae by ectopic Atoh1 expression. PLoS One. 2014;9(2):e89377. [PubMed: 24586731]
55. Liu Z, Walters BJ, Owen T, et al. Regulation of p27Kip1 by Sox2 maintains quiescence of inner pillar cells in the murine auditory sensory epithelium. J Neurosci 2012;32(31):10530–10540. [PubMed: 22855803]
56. Huang LC, Thorne PR, Housley GD, Montgomery JM. Spatiotemporal definition of neurite outgrowth, refinement and retraction in the developing mouse cochlea. Development. 2007;134(16):2925–2933. [PubMed: 17626062]
57. Burda H, Branis M. Postnatal development of the organ of corti in the wild house mouse, laboratory mouse, and their hybrid. Hear Res 1988;36(1):97–105. [PubMed: 3198524]
58. Li Y, Jia S, Liu H, et al. Characterization of hair cell-like cells converted from supporting cells after notch inhibition in cultures of the organ of corti from neonatal gerbils. Front Cell Neurosci 2018;12:73. [PubMed: 29662441]
59. Gubbels SP, Woessner DW, Mitchell JC, Ricci AJ, Brigande JV. Functional auditory hair cells produced in the mammalian cochlea by in utero gene transfer. Nature. 2008;455(7212):537–541. [PubMed: 18754012]
60. Lowenheim H, Furness DN, Kil J, et al. Gene disruption of p27(Kip1) allows cell proliferation in the postnatal and adult organ of corti. Proc Natl Acad Sci U S A 1999;96(7):4084–4088. [PubMed: 10097167]
61. Walters BJ, Liu Z, Crabtree M, Coak E, Cox BC, Zuo J. Auditory hair cell-specific deletion of p27Kip1 in postnatal mice promotes cell-autonomous generation of new hair cells and normal hearing. J Neurosci 2014;34(47):15751–15763. [PubMed: 25411503]
62. Kuo BR, Baldwin EM, Layman WS, Taketo MM, Zuo J. In vivo cochlear hair cell generation and survival by coactivation of beta-catenin and Atoh1. J Neurosci 2015;35(30):10786–10798. [PubMed: 26224861]
63. Liu Z, Dearman JA, Cox BC, et al. Age-dependent in vivo conversion of mouse cochlear pillar and deiters' cells to immature hair cells by Atoh1 ectopic expression. J Neurosci 2012;32(19):6600–6610. [PubMed: 22573682]
64. Kawamoto K, Ishimoto S, Minoda R, Brough DE, Raphael Y. Math1 gene transfer generates new cochlear hair cells in mature guinea pigs in vivo. J Neurosci 2003;23(11):4395–4400. [PubMed: 12805278]
65. Richardson RT, Atkinson PJ. Atoh1 gene therapy in the cochlea for hair cell regeneration. Expert Opin Biol Ther 2015;15(3):417–430. [PubMed: 25648190]
66. Zheng JL, Shou J, Guillemot F, Kageyama R, Gao WQ. Hes1 is a negative regulator of inner ear hair cell differentiation. Development. 2000;127(21):4551–4560. [PubMed: 11023859]
67. Izumikawa M, Minoda R, Kawamoto K, et al. Auditory hair cell replacement and hearing improvement by Atoh1 gene therapy in deaf mammals. Nat Med 2005;11(3):271–276. [PubMed: 15711559]
68. Luo WW, Han Z, Ren DD, Wang XW, Chi FL, Yang JM. Notch pathway inhibitor DAPT enhances Atoh1 activity to generate new hair cells in situ in rat cochleae. Neural Regen Res 2017;12(12):2092–2099. [PubMed: 29323051]
69. Li W, Wu J, Yang J, et al. Notch inhibition induces mitotically generated hair cells in mammalian cochleae via activating the wnt pathway. Proc Natl Acad Sci U S A 2015;112(1):166–171. [PubMed: 25535395]

70. Mizutari K, Fujioka M, Hosoya M, et al. Notch inhibition induces cochlear hair cell regeneration and recovery of hearing after acoustic trauma. Neuron 2013;77(1):58–69. [PubMed: 23312516]

71. Pan W, Jin Y, Stanger B, Kiernan AE. Notch signaling is required for the generation of hair cells and supporting cells in the mammalian inner ear. Proc Natl Acad Sci U S A 2010;107(36):15798–15803. [PubMed: 20733081]

72. Abdolazimi Y, Stojanova Z, Segil N. Selection of cell fate in the organ of corti involves the integration of hes/hey signaling at the Atoh1 promoter. Development. 2016;143(5):841–850. [PubMed: 26932672]

73. Tateya T, Imayoshi I, Tateya I, Ito J, Kageyama R. Cooperative functions of hes/hey genes in auditory hair cell and supporting cell development. Dev Biol 2011;352(2):329–340. [PubMed: 21300049]

Highlights

- Combined suppression of the three retinoblastoma family genes (i.e., Rb1, Rbl1/p107, and Rbl2/p130) through transient overexpression of CycD1 in the inner ear leads to supernumerary cells
- Supernumerary cells were concentrated at the inner hair cells' (IHCs) region
- No signs of apoptosis are observed up to P48
- Auditory and vestibular phenotypes showed no significant signs of abnormality.

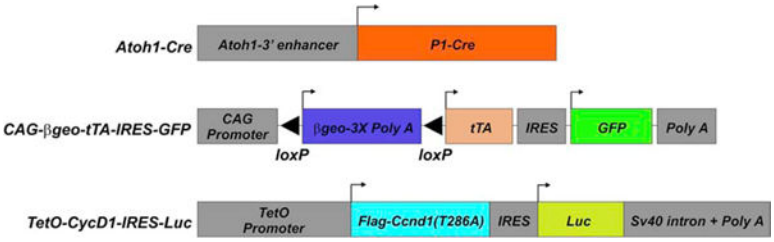

Fig 1. The making of the *Atoh1-Cre*$^{+}$*;CAG-βgeo-tTA-IRES-GFP*$^{+}$*;TetO-CycD1-IRES-Luc*$^{+}$ *(ACTTD1)* mouse model.

Breeding of the *Atoh1-Cre*[30] to the *CAG-βgeo-tTA-IRES-GFP*[31] mouse allow for *Cre*-mediated *loxP* recombination, removal of a transcriptional *3x poly A* (stop) sequence located between the *βgeo* promoter and the *tTA* coding sequence, and activation of the tetracycline-controlled transactivator (*tTA*, Tet-OFF) and downstream GFP reporter. Further breeding of the *Atoh1-Cre; CAG-βgeo-tTA-IRES-GFP* to the *TetO-CycD1-IRES-Luc*[36] unleashes activation and overexpression of the CycD1 transgene.

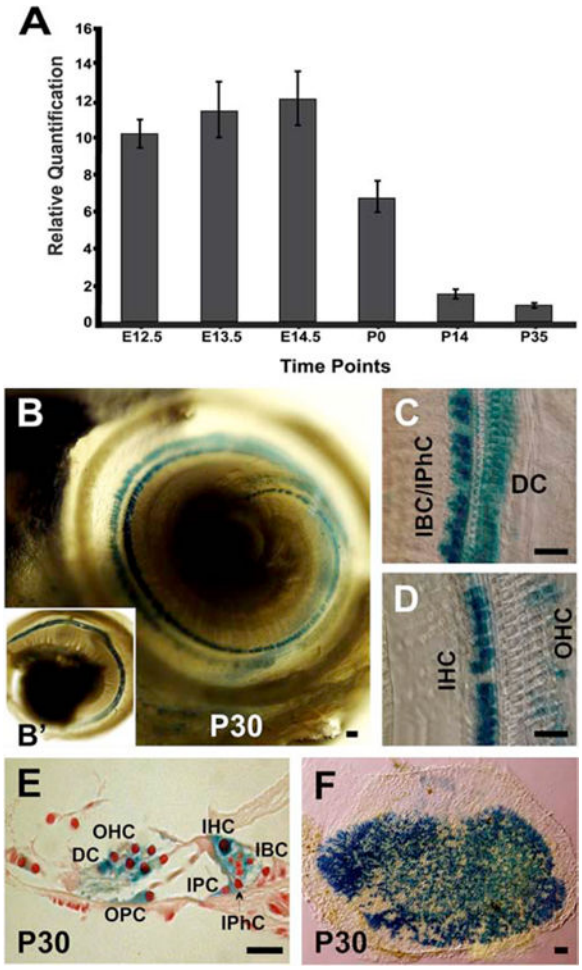

Fig 2. CycD1 and *CAG-βgeo-tTA* expression in the WT inner ear.

(**A)** Endogenous CycD1 expression in the developing and postnatal inner ear. (**B-F)** Specific *CAG-βgeo-tTA-GFP* expression in a P30 mouse cochlea (**B-E**) and vestibular sensory epithelia (**F**). Error bars in (A) correspond to the standard deviations of the relative expression ($2^{-(\Delta\Delta CT +/- \text{pooled StDev})}$) of CycD1' and *β-Actin's* CT values. OHC = outer hair cells; IHC = inner hair cells; DC = Deiters' cells; OPC = outer pillar cells; IPC = inner pillar cells IBC = inner border cells; IPhC = inner phalangeal cells. Bar = 10μm.

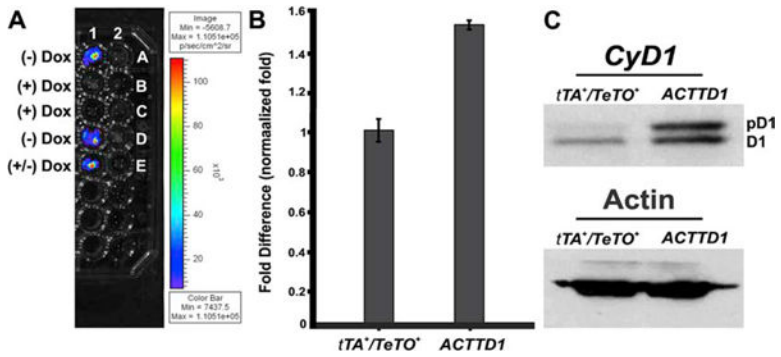

Fig 3. *In vitro* qualitative assessment of combined the *ACTTD1* transgene responsiveness to Dox treatment.

(A) Bioluminescence analysis of triple-positive *ACTTD1* mice cochleae (lane 1) and age-matched negative controls lacking *Atoh1-Cre* (lane 2) at different postnatal time points. Positive luciferase activity was detected in non-Dox-treated *ACTTD1* cochleae at P12 (lane 1, well A), and P26 (lane 1, row D), but not on age-matched, Dox-treated *ACTTD1* animals (lane 1, wells B, C, respectively). Negative control animals displayed no luciferase activity regardless of the absence (lane 2, wells A, D) or presence (lane 2, wells B, C) of Dox. Confirming the transgene's tight regulation, P48 mice, previously treated with Dox for ten days to suppress transgene activity, showed full transgene reactivation 17 days after Dox suppression (lane 1, well E). Of note, no changes were observed in the age-matched negative control cochlea lacking *Atoh1-Cre* (lane 2, well E). **(B, C)** Further supporting efficient *CAG-βgeo-tTA-GFP* transactivation, both CycD1 transcript (**B**) and protein (**C**) were upregulated in the adult *ACTTD1* OC. D1 = unphosphorylated CycD1; pD1 = phosphorylated (active) CycD1.

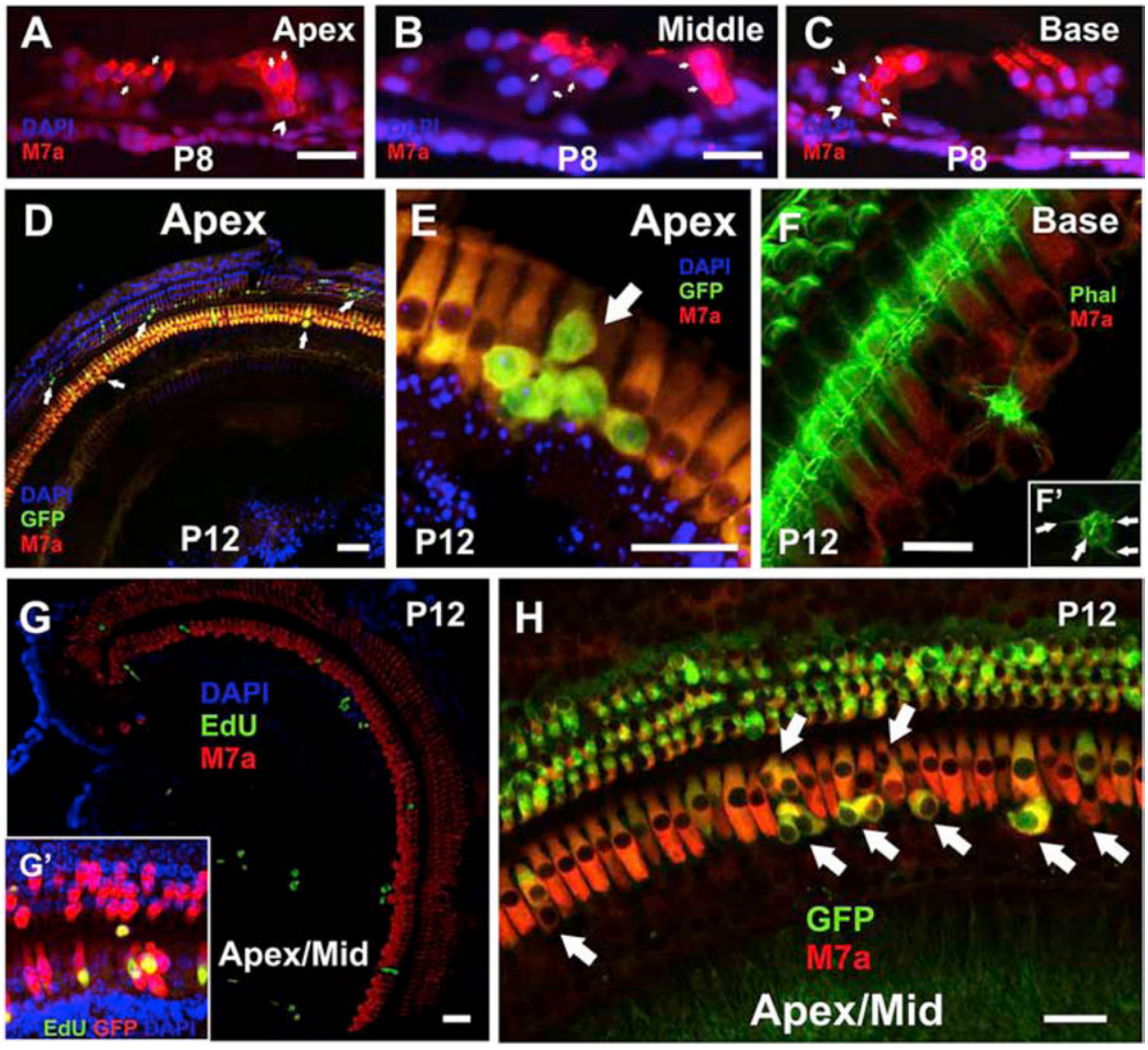

Fig 4. Supernumerary cells in the P8 and P12 *ACTTD1* mouse cochlea.

(A-C). Sections of the different regions of the OC display supernumerary cells in both OHC and IHC regions. **(D).** The location of those supernumerary cells seemed to overlap with that of the GFP^+ (recombined) cells, which were observed in both OHC and IHC regions throughout the length of the *ACTTD1* mouse cochlea. **(E-F').** Supernumerary cells expressed the HC marker M7a and displayed phalloidin-positive apical projections. In many instances, those clusters of supernumerary cells remained attached by their apical projections, forming flower-like structures. **(G-H)**. Consistent with a mitotic origin, EdU-positive nuclei were observed along the length of the cochleae in the proximity of the GFP^+ cells **(G')**. Although GFP+ cells were present in both OHCs' and IHCs' region, most proliferation was observed around the IHCs (**G, G'**). Further supporting their origin and ability to differentiate, postmitotic, supernumerary cells co-expressed GFP and M7a (**D-F, H**). Bar = 20μm (**A-D, G**), 10μm (**F, H**).

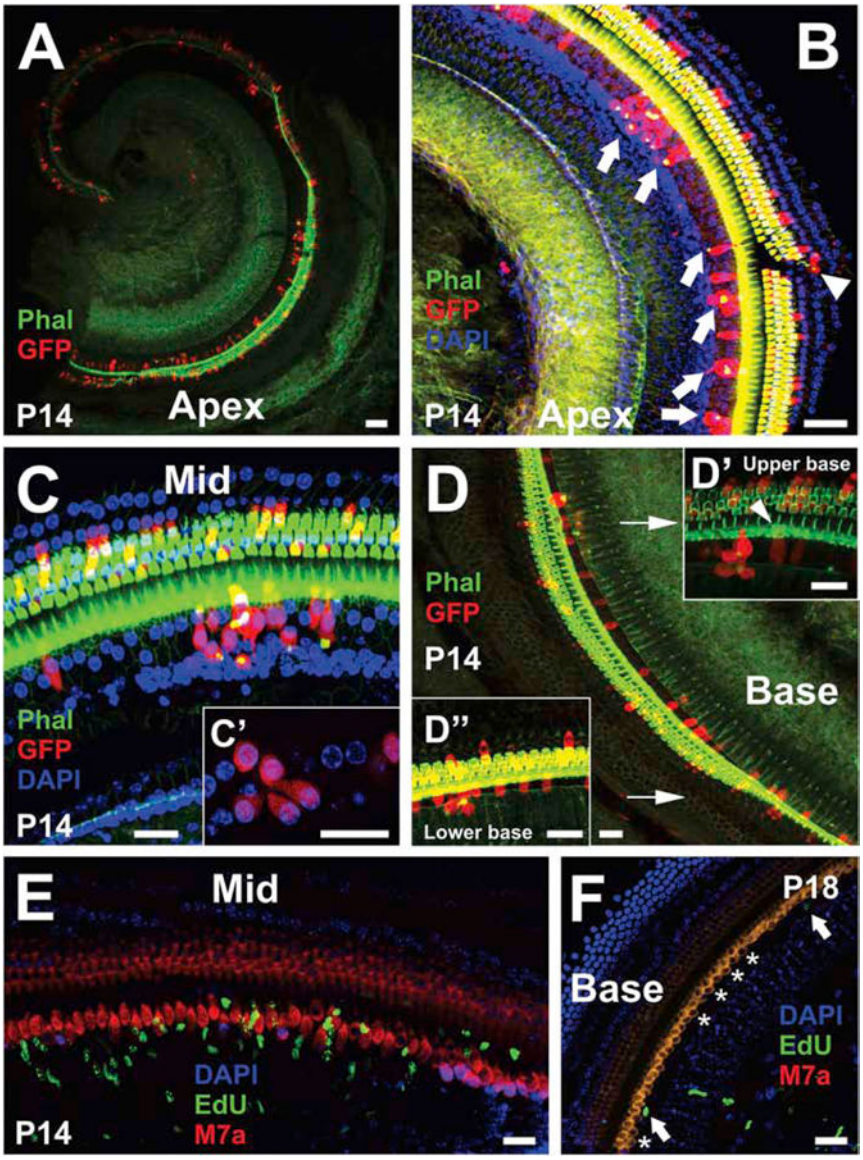

Fig 5. Supernumerary cells in the P14, P18 *ACTTD1* mouse cochleae.

(A-D'') Supernumerary, GFP^{+} supernumerary cells were still observed at P14 and P18 (**E, F**). Similar to earlier time points, the supernumerary cells were mostly arranged in a flower-like structure (**C'**), particularly noticeable near the IHCs' region (in the IPhC, and IB region), and displayed phalloidin-positive apical projections. (**E, F**). Like with earlier time points, proliferative (EdU-positive) cells were also observed at P14. By P18, the presence of proliferative cells was noticeably reduced (**F**). noteworthy, postmitotic supernumerary HCs were still observed and expressed M7a at similar levels as the regular IHCs (**F**, asterisk). Bar = 20μm (**A, B**); 10μm (**C-F**).

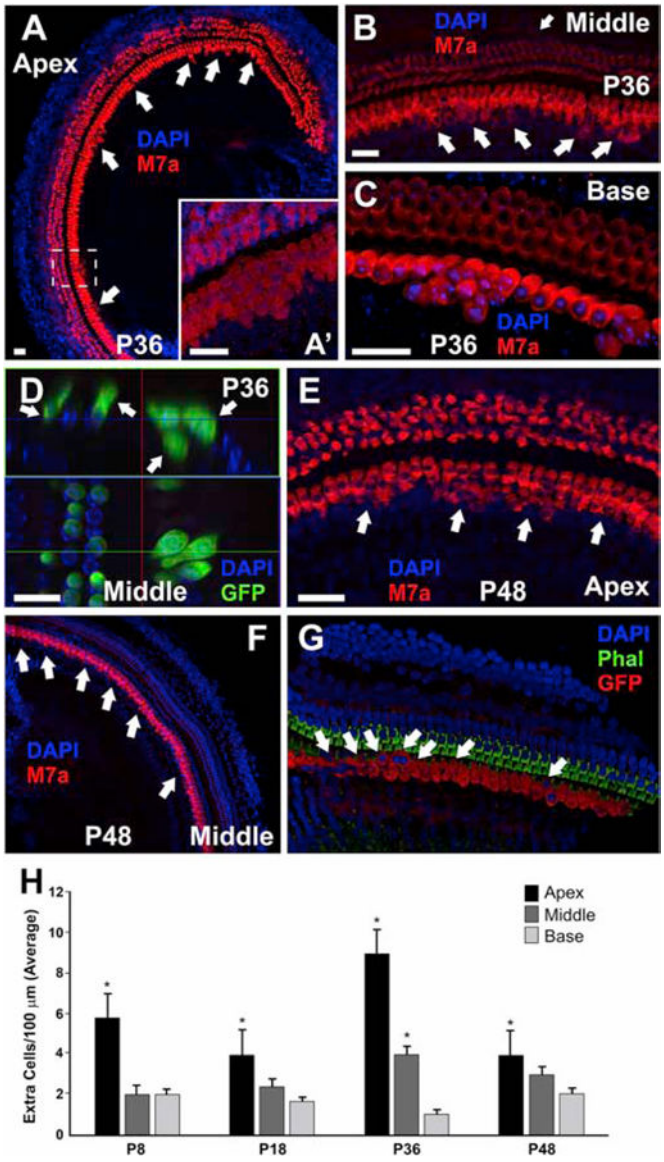

Fig 6. Supernumerary cells in the *ACTTD1* mouse cochleae were still detected at later postnatal time points.

(A-G) Although no signs of cell proliferation were observed at P36 (**A-D**) and P48 (**E-G**), supernumerary, M7a-positive cells were still observed in the apex (**A, A'**), middle (**B**), and basal (**C**) turns of the *ACTTD1* mouse cochleae. (**D**) orthogonal view from different planes (x, y, z) of an area of the confocal microscope image of the apical turn (horizontal green line) once more confirmed the location of the recombined, GFP-positive as well as supernumerary cells near the regular HCs set (arrows). **(E-G)** Except for the apical turn (**E**), where supernumerary cells still looked scattered and disorganized, most supernumerary cells in the middle (F) and basal turns of the *ACTTD1* mouse cochlea were arranged in a single row (arrows) alongside the HCs of the regular set. (**H**) Quantification of supernumerary Myosin VIIa-and GFP-positive cells in the *ACTTD1* mice cochleae at different time points revealed an overall increase in cell numbers in all three turns of the cochlea, but particularly in the apical turn independent of the animal age. The error bars represent the standard

deviations for the mean apex, middle, and base HC differences between *ACTTD1* and WT mice at P8, P18, P36, and P48 from 6 different cochleae per genotype and time point. Statistical significances correspond to differences in cell numbers between the different locations in the cochleae of *ACTTD1* mice at different time points as determined by a Two-way ANOVA (Age X location) with Bonferroni's correction for multiple comparisons. * $P < 0.05$. Bar = 10μm.

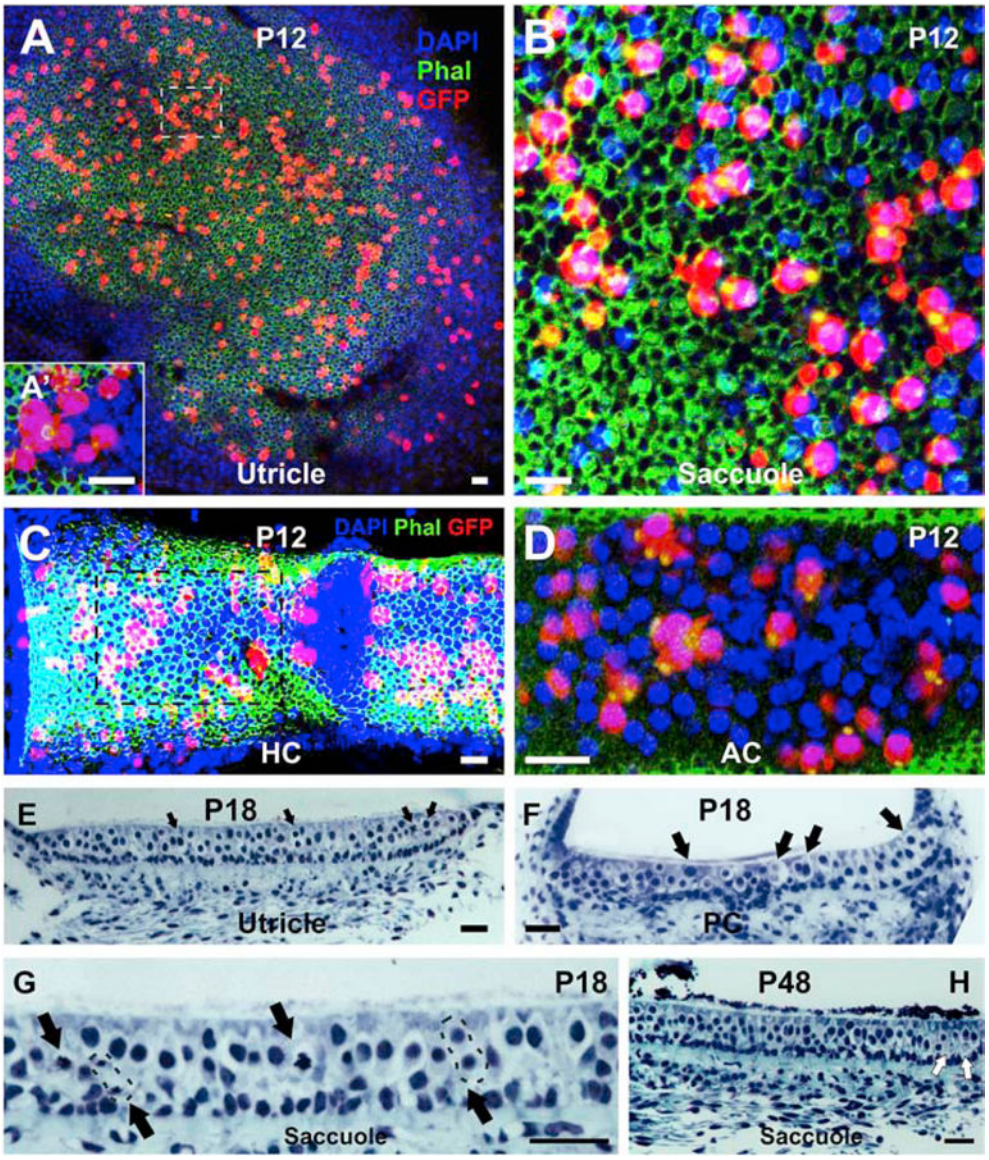

Fig 7. Supernumerary cells in the postnatal *ACTTD1* mouse vestibular end organs

(A-D) At P12 GFP-positive (red) and supernumerary cells were observed dispersed throughout the vestibular end-organs' sensory epithelia. Like the supernumerary cells surrounding the IHCs, the extra cells observed in the vestibular sensory epithelia were mostly arranged in clusters, forming flower-like structures (**A', D**). (**E-F**) Further supporting their mitotic origin, toluidine blue, semi-thin (0.5 μm thick) sections of P18 *ACTTD1* mouse vestibular sensory epithelia displayed proliferating cells at different phases of the cell cycle. Dotted lines in (**G**) highlight mitotic cells. Bar = 10μm.

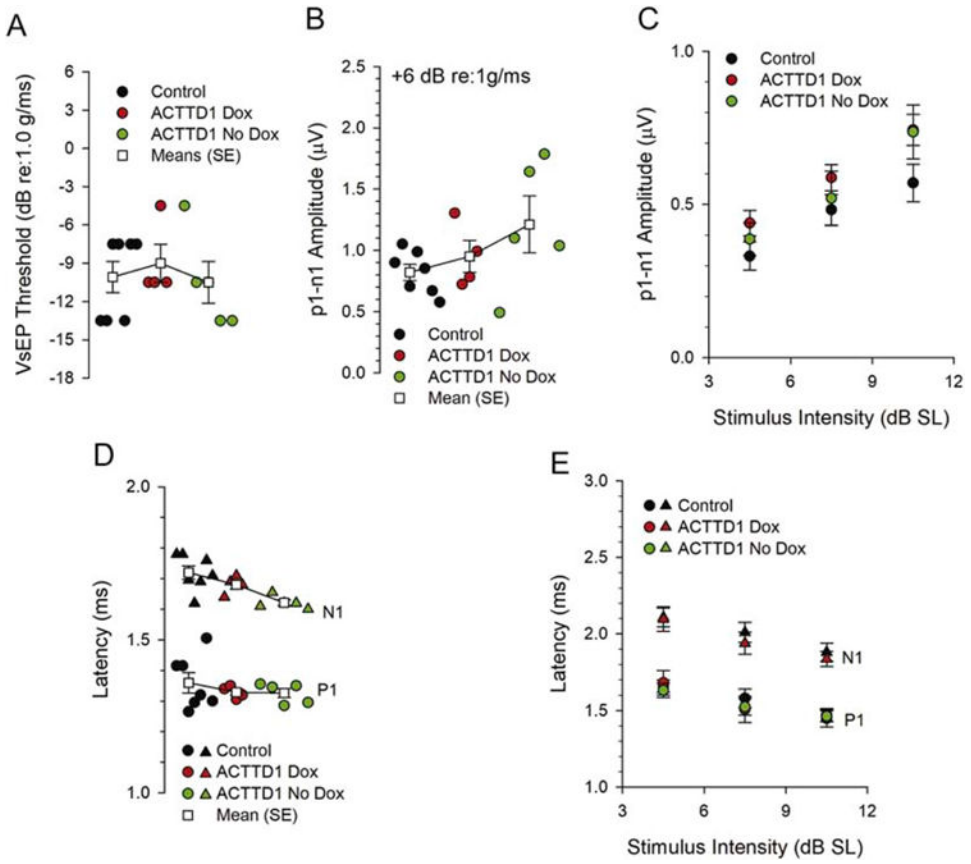

Fig 8. Vestibular sensory-evoked potential (VsEP) responses of control and ACTTD1 mice.

(A) VsEP threshold distributions for control (black circles), ACTTD1 mice treated with Dox (red circles) and untreated ACTTD1 mice (green circles). Means (open squares) and SE are shown for each group. No significant differences were noted between the three groups. **(B)** At the highest stimulus level (+6dB re: 1g/ms), VsEP amplitude (p1-n1) was similar between the three groups. **(C)** VsEP input/output (IO) function where response amplitudes (p1–n1) are plotted as a function of stimulus level in dB SL for control, ACTTD1 mice treated or untreated with Dox. **(D)** At the highest stimulus level (+6dB re: 1g/ms) VsEP latencies (p1, n1) were also similar between the three groups. **(E)** VsEP IO function where response latencies (p1, n1) are plotted as a function of stimulus level in dB SL for the three groups. All three groups showed similar VsEP response characteristics over a wide range of stimulus levels.

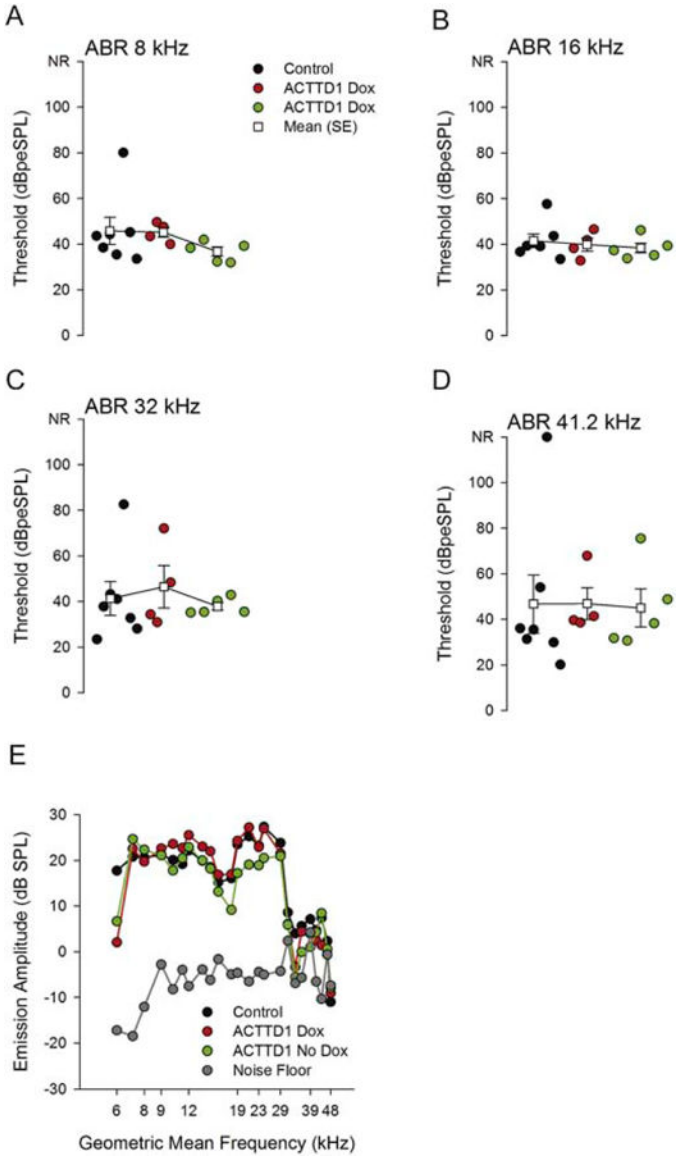

Fig 9. Auditory function in control and ACTTD1 mice.

(A-D) Auditory brainstem response (ABR) threshold distributions in dB peSPL are represented for control and treated/untreated ACTTD1 mice. **(E)** Distortion-product otoacoustic emission (DPOAE) amplitudes. Frequency plotted is the geometric mean of f_1 and f_2. The solid gray line represents the mean noise floor measured across all studies. Black circles – control, red circles – Dox treated ACTTD1, green circles – untreated ACTTD1. There were no significant differences in ABR thresholds of DPOAE amplitudes between the three groups.

Appendix 2

Appendix 2

43RD ANNUAL
MidWinter Meeting

January 25 - 29, 2020

San Jose McEnery Convention Center

San Jose

CALIFORNIA

Results
There was decrease of total hair cell count in the EIT explants compared with control group. We identified the dosage of L-NAC, and Dex together for survival of at least 50% protection of hair cells *in vitro*. This combination therapy may be beneficial in other type of inner ear trauma that can result in hair cell loss.

Conclusion
EIT involves oxidative stress and lipid peroxidation early on after the implantation. L-NAC, and Dex are effective alone in protecting the sensory cells *in vitro* at high doses. A combination containing L-NAC, and Dex at much lower doses of each compound, is effective in protecting sensory cells. These compounds can be combined with synergistic effect allowing a decrease of potential side effects of each compound and providing significant otoprotection for EIT.

PS 946

Does Overexpression of the Transcription Factor Pou4f3 Protect Against Noise-induced Hearing Loss?

Jarnail Singh[1]; Michelle R. Randle[1]; Chantz A. Pinder[1]; Luyi Zhou[1]; Brandon C. Cox[2]
[1]Southern Illinois University, School of Medicine; [2]Departments of Pharmacology & Otolaryngology, Southern Illinois University, School of Medicine

Sensory hair cells are killed by multiple insults including exposure to excessive noise, ototoxic drugs, and ageing. The irreversible loss of hair cells in the mammalian cochlea results in permanent sensory neural hearing loss. Recent studies have shown that overexpression of *Atoh1, Islet1, HSP70,* and neurotrophin genes protects or restores hearing function, hair cells, and/or synapses in the adult cochlea. Here, we investigated the possible role of *Pou4f3* to protect hearing and hair cells from noise exposure. We used tamoxifen inducible *Prestin^{CreERT2}:CAG loxP-stop-loxP-Pou4f3-IRES-mCherry* mice to overexpress *Pou4f3* in outer hair cells (OHCs) at 4 weeks of age. Baseline auditory brainstem responses (ABRs) were performed one day prior to noise exposure (8-16 kHz broadband noise at 105 dB SPL for 1 hour), which was given at 5 weeks of age. Hearing function was then evaluated by ABR at either 1 or 2 weeks after noise exposure, followed by temporal bone collection for assessment of hair cell death. OHCs were manually quantified from confocal images of whole-mount cochlear turns immunostained with an anti-myosin VIIa antibody, and Cre-negative littermates were used as controls. Preliminary ABR results at 1 and 2 weeks post-noise exposure show some protection in mice with *Pou4f3* overexpression at 12 kHz, but not at other frequencies tested. Interestingly, there appears to be increased numbers of OHCs in mice with *Pou4f3* overexpression in all turns of the cochlea at 1 week post-noise exposure compared to controls. However, at 2 weeks after noise exposure, there are no differences in the number of OHCs between controls and mice with *Pou4f3* overexpression. While these preliminary data suggest that overexpression of *Pou4f3* might have limited otoprotective effects, there was variable responses among samples and across genders that needs further investigation. In addition, it is well known that inner hair cells (IHCs) are more resistant to multiple insults as compared to OHCs, and studies have shown that *Pou4f3* is expressed at a higher level in IHCs. Therefore, we are also investigating whether reduced *Pou4f3* expression in IHCs makes them more vulnerable to noise exposure.

Funding: NIH/NIDCD R01 DC014441

PS 947

Quinoxaline, its Derivatives, and Application in Otoprotection

Sonia Rocha-Sanchez[1]; Umesh Pyakurel[1]; Shikha Tarang[1]; Santanu Hati[2]; Hazel Taylor[3]; David Z. He[2]; Huizhan Liu[2]; Jian Zuo[4]; Marisa Zallocchi[2]
[1]Creighton University School of Dentistry; [2]Creighton University School of Medicine; [3]Creighton University; [4]Department of Biomedical Science, Creighton University

As society becomes more technologically advanced, the source of noise pollution and availability of ototoxic are rapidly increasing, posing a threat to our hearing health. Although the underlying mechanism by which these compounds affect auditory function varies, they share common intracellular byproducts, particularly the generation of reactive oxygen species (ROS). This knowledge added to recent advancements in our understanding of oxidative stress and its role in hair cell death has led to the rise of a host of antioxidants as potential therapeutic targets. However, to this date, none of these agents are FDA-approved for otoprotection use. Likewise, the spectrum of otoprotective activity of these agents is unknown. Previous studies support the chemoprotective and therapeutic potential of quinoxaline (Qx), a non-steroidal anti-inflammatory compound, to prevent and treat ototoxin-induced hair cell death. Previous in vitro and zebrafish studies supports Qx's variable chemoprotective effect several against several aminoglycoside antibiotics and full protection against cisplatin. To assess Qx's impact in vivo in a mammalian system, we conducted histological and physiological assessments in wild type (WT) C57BL/6J mice treated

Appendix 3

Appendix 3

43RD ANNUAL
MidWinter Meeting

January 25 - 29, 2020

San Jose McEnery Convention Center

San Jose

CALIFORNIA

to decreased levels of NADPH and glutathione causing abnormal ROS accumulation and oxidative damage, which might trigger apoptosis signal in hair cells and SGNs in Idh2$^{-/-}$ mice. We performed ex vivo experiments to determine whether administration of mitochondria-targeted antioxidants might protect or induce recovery of cells from ROS-induced apoptosis in Idh2-deficient mouse cochlea. MitoQ almost completely neutralized the H2O2-induced ototoxicity, as the survival rate of Idh2$^{-/-}$ hair cells were restored to normal levels. In addition, the lack of IDH2 led to the accumulation of mitochondrial ROS and the depolarization of $\Delta\Psi_m$, resulting in hair cell loss. In the present study, we identified that IDH2 is indispensable for the functional maintenance and survival of hair cells and SGNs. Moreover, the hair cell degeneration caused by IDH2 deficiency can be prevented by MitoQ, which suggests that Idh2$^{-/-}$ mice could be a valuable animal model for evaluating the therapeutic effects of various antioxidant candidates to overcome ROS-induced hearing loss.

PS 451

Quinoxaline protects hair cells from noise-induced damage

Marisa Zallocchi[1]; Jian Zuo[2]; Santanu Hati[1]; Sonia Rocha-Sanchez[3]; Umesh Pyakurel[3]; Shikha Tarang[3]
[1]Creighton University School of Medicine; [2]Department of Biomedical Science, Creighton University; [3]Creighton University School of Dentistry

Hair cell death is the leading cause of hearing and balance disorders in humans. It can be caused by multiple insults, including noise, aging, and treatment with certain therapeutic drugs. As society becomes more technologically advanced, the source of noise pollution and availability of ototoxic drugs are rapidly increasing, posing a threat to our hearing health. While this knowledge has fueled the scientific enthusiasm towards the development of pharmacological interventions, establishing therapeutic measures that slow the progression of hearing loss and protect hearing is still a major clinical challenge. Previous findings from our laboratory have underscored the therapeutic potential of quinoxaline (Qx) and some of its derivatives, to protect the inner ear from cisplatin and aminoglycoside ototoxicity and potentially treat hearing loss. The present study was designed to further expand our current knowledge on the otoprotective effects of Qx and its mechanism of action in hair cells. For this purpose, mice were treated with saline solution or a single intraperitoneal dose of Qx and 24 hours later exposed to an 8-16 kHz octave band noise for 1 hour at 103 dB SPL. Auditory brainstem responses (ABRs) were measured before Qx administration, immediate after noise-exposure or 7 days after noise treatment. While animals treated with saline solution showed threshold shifts of 20 dB or more after 7 days post-noise, ABRs from mice pre-treated with Qx did not show any differences compare to non-noise exposed animals. These results suggest that Qx not only can protect hair cells from drug-induced ototoxicity but also can prevent noise-induce hearing loss. Elsewhere in the body, Qx is known to block NF-kB signaling by inhibiting IKKb and preventing NF-kB nuclear translocation, thereby deterring inflammation and apoptosis. We decided to address whether Qx is targeting the same signaling cascade in hair cells. For this purpose, experiments were performed in HEI-OC1 cells and in transgenic zebrafish lines as well as zebrafish morphants. Results from these experiments suggest that NF-kB pathway is the main target for Qx therapeutic effect. Collectively, the results presented here demonstrated the potential beneficial effect of Qx against noise induced damage, through the regulation of NF-kB and other associated pathways.

Support: NIH 5P20RR018788, R21OD019745-01A1 and 5R01DC015010-04

PS 452

Drug-Induced Hearing Loss Prevention through Clinical Data Driven Drug Re-purposing

Dong Xu; Shaikh Emdadur Rahman; Yuying Huang
Idaho State University

Platinum-based antineoplastic drug and aminoglycoside antibiotics cause irreversible hearing damage or hearing loss. In-vitro studies showed that certain antidepressant agents, HMG-CoA reductase inhibitors (aka statins), and proton pump inhibitors may have protective effects against drug-induced hearing loss (DIHL). A cross-sectional observational study was conducted to evaluate the effect of combinational use of antidepressants with ototoxic drugs using de-identified clinical data obtained from FDA Adverse Events Reporting System. MedDRA PT terms related to DIHL were used to identify the ototoxic events. Among these events, individuals taking any of the 10 ototoxic drugs were considered as the exposed group, while individuals taking any drug from the 32 antidepressants concomitantly with 1 ototoxic drug were put into the outcome group. By calculating the adjusted odds ratio of each drug combination, our study suggests that fluoxetine significantly reduce the ototoxicity of carboplatin (combination aOR 0.03, CI 0.01-0.05, $p < 0.05$, vs Carboplatin aOR 0.80, CI 0.65-0.97, $p < 0.005$). citalopram is found to reduce tobramycin induced ototoxicity significantly (aOR 0.08, CI 0.03-0.17, $p < 0.05$, vs tobramycin aOR 0.198152, CI 0.24-0.16, $p < 0.05$). Atorvastatin shows strong evidence of preventing ototoxic effects. The unadjusted odds ratio

Appendix 4

Pharmacologic Regulation of Auditory Hair Cell Regeneration

W81XWH-20-1-0789
RH190008

PI: Sonia M. Rocha-Sanchez **Org:** Creighton University **Award Amount:** $363,750

Study/Product Aim(s)

SA1: Improve quinoxaline (Qx) efficacy in promoting SC proliferation and differentiation into new HCs through medicinal chemistry, structure-activity relationship (SAR), and *in vivo* pharmacokinetics (PK) and pharmacodynamics (PD).

SA2: Optimize a Qx's oral delivery method to stimulate HC regeneration and characterize its PK/PD properties in the mouse cochleae.

Approach

During the past year, we have designed and conducted experiments described on Specific Aim 1 of our original proposal. Specifically, we have modified our original Qx molecule to generate several new analogs. The analogs were tested *in vitro* (HEI-OC1 cells) and those showing the selection properties (i.e., IC_{50} lower than original Qx's IC_{50}, Water solubility at pH 7.4 and stability in solution with $t_{1/2}$ >4 hours, and showing a balance between IC_{50}, potency, efficacy, and ADMET parameters) were tested *in vitro* (cochlear explants) and *in vivo* (zebrafish).

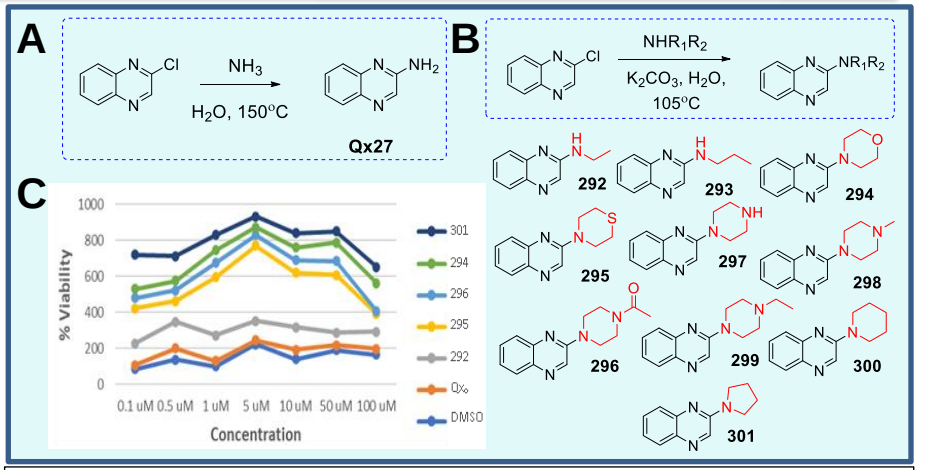

A. Qx-27 is a potent small molecule analog of our lead proliferative drug, Qx. It is a synthetically tractable small molecule ideal for further preclinical optimization. **B.** Synthesis of alkylated Qx-27 analogs. **C.** Proliferative profile of alkylated QX-27 derivatives on HEI-OC1 cells. Controls consisted of the original Qx compound (Qx_o) and DMSO. Qx-294, Qx-295, Qx-296, and Qx-301 showed over 400% cell viability at all concentrations..

Timeline and Cost

Activities CY	20-21	21	22	
Modification of Qx original structure				
Generation of new Qx analogs				
In vitro and *in vivo* testing of new analogs				
Identify the best oral dosage for Qx in vivo				
Estimated Budget ($K)	**$181,875**	**$181,875**		

Updated: (09/15/2021)

Goals/Milestones

Cy20 Goal – To obtain Qx analogs with the following pharmacologic characteristics:

- ☑ IC_{50} lower than original Qx's IC_{50} (ideally in the nM range)
- ☑ Water solubility at pH 7.4, and stability in solution with $t_{1/2}$ >4 hours
- ☑ Show a balance between IC_{50}, potency, efficacy, and ADMET parameters (i.e., absorption, distribution, metabolism, excretion, and toxicity)

Cy21 Goals – *In vivo* testing of Qx's top analogs

- ☑ To test Qx top analogs' potency (IC_{50}) and toxicity (LD_{50}) in mouse cochlear explants
- ☐ *In vivo* Pharmacodynamics (PD) and Pharmacokinetics (PK) assessments (currently in progress)

Cy22 Goal – Production Readiness

- ☐ Randomized PD assessment of multiple concentration, single oral dose Qx treatment in normal-hearing mice
- ☐ Randomized PK assessment of best oral dose determined on subtask 1, at 0.5, 1, 2, 8- and 24-hours post administration

Comments and Challenges: The COVID pandemic and University shutdown/restrictions our timeline is somewhat delayed, particularly the *in vivo* studies.